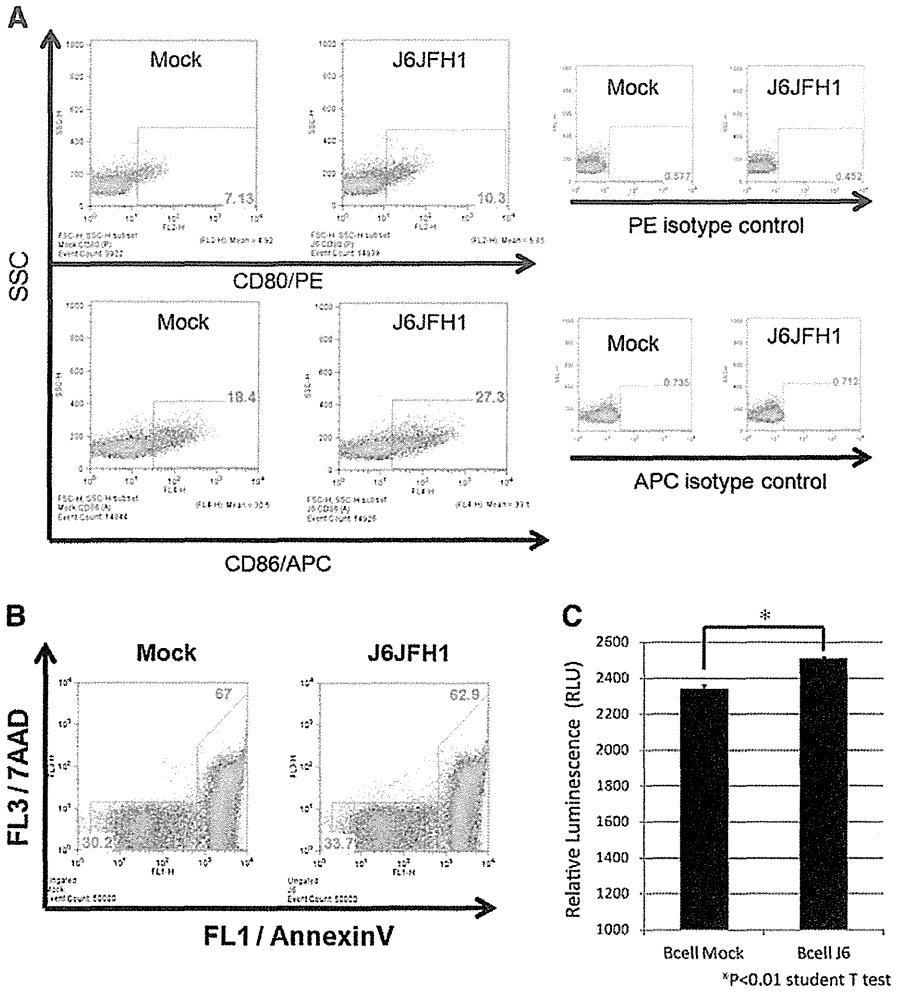

FIG. 6. J6JFH1 infection activates B-cells and protects the cells from apoptosis. Human B-cells were infected with J6JFH1 at MOI = 1 for 3 h, washed twice with PBS, and cultured. Two days after inoculation, cells were washed and suspended with FACS buffer. **(A)** The cells were incubated with PE-conjugated anti-human CD80 antibody, APC-conjugated CD86 antibody, or PE/APC-conjugated mouse IgG1 isotype control for 30 min. Then, the cells were washed and resuspended in FACS buffer. Cells were analyzed by FACS. **(B)** Annexin V and 7AAD viaprobe were added and cultured at 18°C for 10 min. Then, cells were analyzed by FACS. **(C)** 2×10^5 human B-cells were infected with J6JFH1- or Mock-concentrated medium for 3 h. Cells were then washed, resuspended, and cultured in a 96-well white microwell plate. Two days later, ATP activity was determined with a CellTiter-Glo® Luminescent Cell Viability Assay Kit (Promega). ATP activity was adjusted by day 0 ATP activity.

RIG-I and MDA5 in B-cells might recognize HCV RNA and evoke intracellular signaling, including by transcription factors NF-κB and IRF-3/7 (5). Activation of the cytokine network is triggered in human B-cells in response to HCV RNA. In fact, host factors liberated by HCV-infecting B-cells have been previously reported in HCV patients (1,12,15,16,52). Although patients' outcomes would be more than we can be predicted from our results, this system would actually benefit the future study on B-cell–virus interaction.

Acknowledgments

We are grateful to Drs. Frank Chisari (Scripps Research Institute, San Diego, CA) for the Huh7.5.1 cells, Takaji Wakita (National Institute of Infectious Diseases, Tokyo) for supplying the J6JFH1 plasmid, and Brett Lindenbach (Yale University, New Haven, CT) for providing us with the pJc1-GLuc2A HCV strain.

This work was supported in part by Grants-in-Aid from the Ministry of Education, Science, and Culture (Specified Project for "Carcinogenic Spiral") and the Ministry of Health, Labor, and Welfare of Japan, and by the Program of Founding Research Centers for Emerging and Reemerging Infectious Diseases, MEXT. Financial support by the Takeda Science Foundation, the Yasuda Cancer Research Foundation, and the Iskra Foundation are gratefully acknowledged.

Author Disclosure Statement

No competing financial interests exist.

References

1. Agnello V, Chung RT, and Kaplan LM. A role for hepatitis C virus infection in type II cryoglobulinemia. N Engl J Med 1992;327:1490–1495.
2. Aizaki H, Morikawa K, Fukasawa M, *et al.* Critical role of virion-associated cholesterol and sphingolipid in hepatitis C virus infection. J Virol 2008;82:5715–5724.
3. Aly HH, Oshiumi H, Shime H, *et al.* Development of mouse hepatocyte lines permissive for hepatitis C virus (HCV). PLoS One 2011;6:e21284.
4. Aly HH, Qi Y, Atsuzawa K, *et al.* Strain-dependent viral dynamics and virus–cell interactions in a novel *in vitro* system supporting the life cycle of blood-borne hepatitis C virus. Hepatology 2009;50:689–696.
5. Aly HH, Shimotohno K, Hijikata M, and Seya T. *In vitro* models for analysis of the hepatitis C virus life cycle. Microbiol Immunol 2012;56:1–9.
6. Asselah T, and Marcellin P. Second-wave IFN-based triple therapy for HCV genotype 1 infection: simeprevir, faldaprevir and sofosbuvir. Liver Int 2014;34:60–68.
7. Bare P, Massud I, Parodi C, *et al.* Continuous release of hepatitis C virus (HCV) by peripheral blood mononuclear cells and B-lymphoblastoid cell-line cultures derived from HCV-infected patients. J Gen Virol 2005;86:1717–1727.
8. Bartosch B, Dubuisson J, and Cosset FL. Infectious hepatitis C virus pseudo-particles containing functional E1-E2 envelope protein complexes. J Exp Med 2003;197; 633–642.
9. Bartosch B, Vitelli A, Granier C, *et al.* Cell entry of hepatitis C virus requires a set of co-receptors that include the CD81 tetraspanin and the SR-B1 scavenger receptor. J Biol Chem 2003;278:41624–41630.
10. Castet V, Fournier C, Soulier A, *et al.* Alpha interferon inhibits hepatitis C virus replication in primary human hepatocytes infected *in vitro*. J Virol 2002;76:8189–8199.
11. Chen Z, Zhu Y, Ren Y, *et al.* Hepatitis C virus protects human B lymphocytes from Fas-mediated apoptosis via E2-CD81 engagement. PLoS One 2011;6:e18933.
12. Donada C, Crucitti A, Donadon V, *et al.* Systemic manifestations and liver disease in patients with chronic hepatitis C and type II or III mixed cryoglobulinaemia. J Viral Hepat 1998;5:179–185.
13. Ebihara T, Shingai M, Matsumoto M, Wakita T, and Seya T. Hepatitis C virus-infected hepatocytes extrinsically modulate dendritic cell maturation to activate T cells and natural killer cells. Hepatology 2008;48:48–58.
14. Evans MJ, von Hahn T, Tscherne DM, *et al.* Claudin-1 is a hepatitis C virus co-receptor required for a late step in entry. Nature 2007;446:801–805.
15. Ferri C, Caracciolo F, Zignego AL, *et al.* Hepatitis C virus infection in patients with non-Hodgkin's lymphoma. Br J Haematol 1994;88:392–394.
16. Frangeul L, Musset L, Cresta P, Cacoub P, Huraux JM, and Lunel F. Hepatitis C virus genotypes and subtypes in patients with hepatitis C, with and without cryoglobulinemia. J Hepatol 1996;25:427–432.
17. Fried MW, Buti M, Dore GJ, *et al.* Once-daily simeprevir (TMC435) with Pegylated interferon and ribavirin in treatment-naïve genotype 1 hepatitis C: the randomized PILLAR Study. Hepatology 2013;58:1918–1929.
18. Harwood NE, and Batista FD. New insights into the early molecular events underlying B cell activation. Immunity 2008;28:609–619.
19. Hsu M, Zhang J, Flint M, *et al.* Hepatitis C virus glycoproteins mediate pH-dependent cell entry of pseudotyped retroviral particles. Proc Natl Acad Sci U S A 2003;100: 7271–7276.
20. Inokuchi M, Ito T, Uchikoshi M, *et al.* Infection of B cells with hepatitis C virus for the development of lymphoproliferative disorders in patients with chronic hepatitis C. J Med Virol 2009;627:619–627.
21. Ito M, Masumi A, Mochida K, *et al.* Peripheral B cells may serve as a reservoir for persistent hepatitis C virus infection. J Innate Immun 2010;2:607–617.
22. Jacobson IM, McHutchison JG, Dusheiko G, *et al.* Telaprevir for previously untreated chronic hepatitis C virus infection. N Engl J Med 2011;364:2405–2416.
23. Jahan S, Khaliq S, Siddiqi MH, *et al.* Anti-apoptotic effect of HCV core gene of genotype 3a in Huh-7 cell line. Virol J 2011;8:522.
24. Kambara H, Fukuhara T, Shiokawa M, *et al.* Establishment of a novel permissive cell line for the propagation of hepatitis C virus by expression of microRNA miR122. J Virol 2012;86:1382–1393.
25. Karavattathayyil SJ, Kalkeri G, Liu HJ, *et al.* Detection of hepatitis C virus RNA sequences in B-cell non-Hodgkin lymphoma. Am J Clin Pathol 2000;113:391–398.
26. Kasama Y, Sekiguchi S, Saito M, *et al.* Persistent expression of the full genome of hepatitis C virus in B cells induces spontaneous development of B-cell lymphomas *in vivo*. Blood 2010;116;4926–4933.
27. Kondo Y, and Shimosegawa T. Direct effects of hepatitis C virus on the lymphoid cells. World J Gastroenterol 2013; 19:7889–7895.
28. Ladu S, Calvisi DF, Conner EA, Farina M, Factor VM, and Thorgeirsson SS. E2F1 inhibits c-Myc-driven apoptosis via PIK3CA/Akt/mTOR and COX-2 in a mouse model of human liver cancer. Gastroenterology 2008;135:1322–1332.
29. Lanford RE, Chavez D, Chisari FV, and Sureau C. Lack of detection of negative-strand hepatitis C virus RNA in peripheral blood mononuclear cells and other extrahepatic tissues by the highly strand-specific rTth reverse transcriptase PCR. J Virol 1995;69:8079–8083.
30. Laskus T, Radkowski M, Wang LF, Vargas H, and Rakela J. The presence of active hepatitis C virus replication in lymphoid tissue in patients coinfected with human immunodeficiency virus type 1. J Infect Dis 1998;178:1189–1192.
31. Lerat H, Berby F, Trabaud MA, *et al.* Specific detection of hepatitis C virus minus strand RNA in hematopoietic cells. J Clin Invest 1996;97:845–851.
32. Lok AS, Gardiner DF, Hézode C, *et al.* Randomized trial of daclatasvir and asunaprevir with or without PegIFN/RBV for hepatitis C virus genotype 1 null responders. J Hepatrol 2014;60:490–499.
33. Lowe SW, and Lin AW. Apoptosis in cancer. Carcinogenesis 2000;21:485–495.
34. MacParland SA, Pham TN, Guy CS, and Michalak TI. Hepatitis C virus persisting after clinically apparent sustained virological response to antiviral therapy retains infectivity *in vitro*. Hepatology 2009;49:1431–1441.
35. Marukian S, Jones CT, Andrus L, *et al.* Cell culture-produced hepatitis C virus does not infect peripheral blood mononuclear cells. Hepatology 2008;48:1843–1850.
36. Mazzaro C, Franzin F, Tulissi P, *et al.* Regression of monoclonal B-cell expansion in patients affected by mixed cryoglobulinemia responsive to alpha-interferon therapy. Cancer 1996;77:2604–2613.

37. McKeating JA, Zhang LQ, Logvinoff C, *et al.* Diverse hepatitis C virus glycoproteins mediate viral infection in a CD81-dependent manner. J Virol 2004;78:8496–8505.
38. Mizuochi T, Ito M, Takai K, and Yamaguchi K. Peripheral blood memory B cells are resistant to apoptosis in chronic hepatitis C patients. Virus Res 2011;155:349–351.
39. Murakami K, Kimura T, Shoji I, *et al.* Virological characterization of the hepatitis C virus JFH-1 strain in lymphocytic cell lines. J Gen Virol 2008;89:1587–1592.
40. Muratori L, Gibellini D, Lenzi M, *et al.* Quantification of hepatitis C virus-infected peripheral blood mononuclear cells by *in situ* reverse transcriptase-polymerase chain reaction. Blood 1996;88:2768–2774.
41. Phan T, Beran RKF, Peters C, Lorenz IC, and Lindenbach BD. Hepatitis C virus NS2 protein contributes to virus particle assembly via opposing epistatic interactions with the E1-E2 glycoprotein and NS3-NS4A enzyme complexes. J Virol 2009;83:8379–8395.
42. Pileri P, Uematsu Y, Campagnoli S, *et al.* Binding of hepatitis C virus to CD81. Science 1998;282:938–941.
43. Ploss A, Evans MJ, Gaysinskaya VA, *et al.* Human occludin is a hepatitis C virus entry factor required for infection of mouse cells. Nature 2009;457:882–886.
44. Qu J, Zhang Q, Li Y, *et al.* The Tat protein of human immunodeficiency virus-1 enhances hepatitis C virus replication through interferon gamma-inducible protein-10. BMC Immunol 2012;13:15.
45. Radkowski M, Gallegos-Orozco JF, Jablonska J, *et al.* Persistence of hepatitis C virus in patients successfully treated for chronic hepatitis C. Hepatology 2005;41:106–114.
46. Ramakrishnaiah V, Thumann C, Fofana I, *et al.* Exosome-mediated transmission of hepatitis C virus between human hepatoma Huh7.5 cells. Proc Natl Acad Sci U S A 2013; 110:13109–13113.
47. Sarhan MA, Pham TNQ, Chen AY, and Michalak TI. Hepatitis C virus infection of human T lymphocytes is mediated by CD5. J Virol 2012;86:3723–3735.
48. Schmidt WN, Stapleton JT, LaBrecque DR, *et al.* Hepatitis C virus (HCV) infection and cryoglobulinemia: analysis of whole blood and plasma HCV RNA concentrations and correlation with liver histology. Hepatology 2000;31: 737–744.
49. Schulze-Bergkamen H, Krammer P.H. Apoptosis in cancer—implications for therapy. Semin Oncol 2004;31: 90–119.
50. Seto WK, Lai CL, Fung J, *et al.* Natural history of chronic hepatitis C: genotype 1 versus genotype 6. J Hepatol 2010; 53:444–448.
51. Sung VM, Shimodaira S, Doughty AL, *et al.* Establishment of B-cell lymphoma cell lines persistently infected with hepatitis C virus *in vivo* and *in vitro*: the apoptotic effects of virus infection. J Virol 2003;77:2134–2146.
52. Turner NC. Hepatitis C and B-cell lymphoma. Ann Oncol 2003;14:1341–1345.
53. Wakita T, Pietschmann T, Kato T, *et al.* Production of infectious hepatitis C virus in tissue culture from a cloned viral genome. Nature Med 2005;11:791–796.

Address correspondence to:
Dr. Tsukasa Seya
Department of Microbiology and Immunology
Hokkaido University Graduate School of Medicine
Kita 15, Nishi 7
Kita-ku
Sapporo 060-8638
Japan

E-mail: seya-tu@pop.med.hokudai.ac.jp

Endosomal Localization of TLR8 Confers Distinctive Proteolytic Processing on Human Myeloid Cells

Noriko Ishii,[1] Kenji Funami,[1] Megumi Tatematsu, Tsukasa Seya, and Misako Matsumoto

Nucleic acid–sensing TLRs are involved in both antimicrobial immune responses and autoimmune inflammation. TLR8 is phylogenetically and structurally related to TLR7 and TLR9, which undergo proteolytic processing in the endolysosomes to generate functional receptors. Recent structural analyses of human TLR8 ectodomain and its liganded form demonstrated that TLR8 is also cleaved, and both the N- and C-terminal halves contribute to ligand binding. However, the structures and ssRNA recognition mode of endogenous TLR8 in human primary cells are largely unknown. In this study, we show that proteolytic processing of TLR8 occurs in human monocytes and macrophages in a different manner compared with TLR7/9 cleavage. The insertion loop between leucine-rich repeats 14 and 15 in TLR8 is indispensable for the cleavage and stepwise processing that occurs in the N-terminal fragment. Both furin-like proprotein convertase and cathepsins contribute to TLR8 cleavage in the early/late endosomes. TLR8 recognizes viral ssRNA and endogenous RNA, such as microRNAs, resulting in the production of proinflammatory cytokines. Hence, localization sites of the receptors are crucial for the nucleic acid–sensing mode and downstream signaling. *The Journal of Immunology*, **2014, 193: 5118–5128.**

Discrimination between self and nonself by the innate immune system is crucial for swift elimination of infectious microbes, as well as protection against autoimmune disorders (1, 2). The compartmentalized pattern recognition receptors, including TLR3, TLR7, TLR8, and TLR9, participate in the recognition of extracellular microbial nucleic acids and transmission of innate immune signaling (3). The nucleic acid–sensing TLRs localize to the endosomal compartments (4, 5), which prevents them from responding to self nucleic acids in steady-states. The endoplasmic reticulum (ER)-resident multispan transmembrane protein UNC93B1 is indispensable for intracellular localization and signaling of these TLRs (6–10). UNC93B1 associates with TLR3, TLR7, TLR8, and TLR9 through transmembrane domains in the ER and promotes intracellular trafficking of those TLRs from the ER to the Golgi. However, the destination of each TLR is regulated by distinct determinants within TLRs (10–13).

TLR7, TLR8, and TLR9 form a subfamily of proteins that shares structural features (14, 15). Their ectodomains (ECDs) consist of 26 leucine-rich repeats (LRRs) with a large insertion loop between LRR14 and LRR15 and N- and C-terminal flanking region, LRRNT and LRRCT (16). Ligand binding to TLR–ECD induces receptor dimerization, allowing access of adaptor molecule MyD88 to the cytoplasmic Toll–IL-1R (TIR) domains (17). TLR7 and TLR8 recognize ssRNA and synthetic imidazoquinoline derivatives (18–21), whereas TLR9 recognizes CpG-containing DNA (22, 23). Accumulating evidence indicates that TLR7 and TLR9 undergo proteolytic processing in the endolysosomes of macrophages and plasmacytoid dendritic cells (pDCs) to generate functional receptors (24–29). The pH-dependent endosomal cathepsins, as well as a cysteine lysosomal protease asparaginyl endopeptidase (AEP), participate in mouse (m)/human (h)TLR9 and mTLR7 cleavage at the loop region, which is necessary for nucleic acid sensing. Hipp et al. (30) also demonstrated that hTLR7 processing is mediated with furin-like proprotein convertase. Although the truncated receptors appear to be signaling competent (26, 29), the N-terminal fragment contributes to full activation of the receptors via association with the C-terminal half (31, 32).

In humans, TLR8 is expressed in myeloid cells, including monocytes, neutrophils, macrophages, and myeloid dendritic cells (DCs), and in regulatory T cells (33–36). TLR8 recognizes viral GU-rich ssRNA and endogenous RNA, such as microRNAs within exosomes, leading to the production of proinflammatory cytokines but not type I IFNs (37, 38). Recent structural analysis of hTLR8 ECD and its ligand complex showed that TLR8 is cleaved as well, and both the N- and C-terminal halves are engaged in ligand recognition (39). However, whether the proteolytic cleavage of endogenous TLR8 actually occurs in human primary cells and how TLR8 undergoes processing remain obscure. In this study, we investigated the cleavage of TLR8 and its requirement for ligand recognition in human primary cells, including monocytes and monocyte-derived macrophages.

Materials and Methods

Cell culture, Abs, and reagents

HEK293 cells were maintained in DMEM low glucose (Invitrogen) supplemented with 10% heat-inactivated FCS (BioSource International) and antibiotics. HEK293FT cells were maintained in DMEM high glucose supplemented with 0.1 mM nonessential amino acids, 10% heat-inactivated FCS, and antibiotics. RAW264.7 cells and THP-1 cells were maintained in RPMI 1640 (Invitrogen) supplemented with 10% heat-inactivated FCS, 55 μM 2-ME (for THP-1 cells), and antibiotics. Human monocytes and B cells were isolated from PBMCs obtained from healthy individuals with a magnetic cell sorting system using anti-CD14–coated and anti-CD19–

Department of Microbiology and Immunology, Hokkaido University Graduate School of Medicine, Sapporo 060-8638, Japan

[1]N.I. and K.F. contributed equally to this work.

Received for publication May 30, 2014. Accepted for publication September 4, 2014.

This work was supported in part by grants-in-aid from the Ministry of Education, Science, and Culture, the Ministry of Health, Labor, and Welfare of Japan, and by the Akiyama Life Science Foundation.

Address correspondence and reprint requests to Dr. Misako Matsumoto, Department of Microbiology and Immunology, Hokkaido University Graduate School of Medicine, Kita 15, Nishi 7, Kita-ku, Sapporo 060-8638, Japan. E-mail address: matumoto@pop.med.hokudai.ac.jp

The online version of this article contains supplemental material.

Abbreviations used in this article: AEP, asparaginyl endopeptidase; DC, dendritic cell; ECD, ectodomain; ER, endoplasmic reticulum; h, human; LRR, leucine-rich repeat; m, mouse; MPR, mannose 6 phosphate receptor; pAb, polyclonal Ab; pDC, plasmacytoid dendritic cell; siRNA, small interfering RNA; TIR, Toll–IL-1R; TLR8-C, TLR8 C-terminal fragment; TLR8Δloop, TLR8 lacking the flexible loop between LRR14 and LRR15; TLR8-N, TLR8 N-terminal fragment.

www.jimmunol.org/cgi/doi/10.4049/jimmunol.1401375

coated MicroBeads (Miltenyi Biotec, Gladbach, Germany), respectively. Purity was checked routinely by FACS and was >95%. Monocyte-derived macrophages were differentiated from $CD14^+$ monocytes by culturing with 20 ng/ml recombinant hGM-CSF (PeproTech) for 6 d. Anti-FLAG M2 mAb, anti-FLAG polyclonal Ab (pAb), brefeldin A, z-FA-FMK, DC1 (3,3′-(5-Indolyl methylene)bis(4-hydroxycoumarin)), and LPS (*Escherichia coli* 0111:B4) were purchased from Sigma-Aldrich. In addition, the following Abs were used in this study: PE mIgG1, PE anti-human CD80 mAb, and PE anti-human CD19 mAb (all from eBioscience); FITC mIgG2b, PE anti-human CD14 mAb, and FITC anti-human CD68 mAb (all from BioLegend); Alexa Fluor– or HRP-conjugated secondary Abs (all from Invitrogen); anti-early endosome Ag 1 rabbit mAb (Cell Signaling Technology Japan); anti-GM130 mAb (BD Transduction Laboratories); anti-calnexin pAb (Stressgen; Victoria, BC, Canada); anti-p115 pAb, anti-mannose 6 phosphate receptor (MPR) pAb, anti-MPR mAb, and anti-calnexin mAb (all from Abcam, Cambridge, U.K.), anti–Lamp-1 mAb and anti–tubulin-α mAb (BioLegend); and anti-hTLR8 rabbit mAb (CST Japan). Affinity-purified rabbit pAb against hTLR8 cytoplasmic region was generated by MBL. LysoTracker Red was purchased from Invitrogen. CL075 was from InvivoGen. ssRNA40 (5′-GCCCGUCUGUUGUGUGACUC-3′, a 20-mer phosphorothioate protected ssRNA oligonucleotide) and biotinylated ssRNA40 were synthesized by Hokkaido System Science (Sapporo, Japan).

Plasmids

cDNAs for hTLR7 and hTLR8 were cloned in our laboratory by RT-PCR from the mRNA of monocyte-derived macrophages and were ligated into the cloning site of the expression vector, pEF-BOS, which was provided by Dr. S. Nagata (Kyoto University). The FLAG tag was inserted into the C terminus of pEF-BOS expression vectors for hTLR7 and hTLR8. The C-terminal FLAG-tagged TLR8 mutant lacking the flexible loop between LRR14 and LRR15 (TLR8 lacking the flexible loop between LRR14 and LRR15 [TLR8Δloop]) and the mutant lacking LRR1–14 and the flexible loop (TLR8 C-terminal fragment [TLR8-C]) were generated by PCR with KOD-Plus DNA polymerase (TOYOBO) using specific primers (forward primer: 5′-TATGGAAAAGCCTTAGATTTAAGCC-3′, reverse primer: 5′-ATAACTCTGCCGGGTATCTTTTACC-3′ for TLR8Δloop; and forward primer: 5′-TATGGAAAAGCCTTAGATTTAAGCC-3′, reverse primer: 5′-TTTGCCCACCGTTTGGGGAACTTCC-3′ for TLR8-C), as described (11). The C-terminal FLAG-tagged TLR8 mutant, R467A/R470A/R472A/R473A, was generated by site-directed mutagenesis using specific primers (forward primer: 5′-GCAGCCTCAACAGATTTTGAGTTTGACCC-3′, reverse primer: 5′-TTTCGCGATATGAGCTTGAAAAGAGGAACTATTTGC-3′). The TLR8 N-terminal fragment (LRR-NT+LRR1–14) (TLR8-N) was generated by PCR using specific primers (forward primer: 5′-CTCGAGCCACCATGAAGGAGTCATCTTTGC-3′ and reverse primer: 5′-AAAGCGGCCGCTTAATAACTCTGCCGGGTATC-3′). pEFBOS/hTLR8-FLAG-IRES-Puromycin and pEFBOS/hTLR8Δloop-FLAG-IRES-Puromycin were made in our laboratory and used for stable expression of hTLR8 and hTLR8Δloop, respectively, in RAW294.7 cells. Plasmids for human UNC93B1 (pMD2/UNC93B1) and hTLR9 (pBluescript II/TLR9) were provided by Dr. K. Miyake (The University of Tokyo) and Dr. S. Akira (Osaka University), respectively. The HA tag and FLAG tag were inserted into the C terminus of the pEF-BOS expression vector for human UNC93B1 and hTLR9, respectively.

Reporter gene assay

HEK293 cells (3×10^4 cells/well), cultured in 96-well plates, were transfected with the indicated plasmid together with the reporter plasmid and an internal control vector, phRL-TK (Promega), using FuGENE HD (Roche). The reporter plasmid containing the ELAM-1 promoter was constructed in our laboratory. Twenty-four hours after transfection, cells were stimulated with CL075 and ssRNA40 complexed to DOTAP (Roche). The cells were collected 12 h after stimulation and lysed. Firefly and *Renilla* luciferase activities were determined using a dual-luciferase reporter assay kit (Promega). The firefly luciferase activity was normalized to the *Renilla* luciferase activity and expressed as the fold induction relative to the activity in unstimulated vector-transfected cells. All assays were performed in triplicate.

RNA interference

Small interfering RNA (siRNA) duplexes (hTLR8: #s27921; negative control: #AM4635) were obtained from Ambion-Applied Biosystems. Human monocytes (5×10^5/ml) were cultured in 24-well plates with 20 ng/ml hGM-CSF. At day 4, cells were transfected with 30 pmol control or TLR8 siRNA using Lipofectamine RNAiMAX (Invitrogen). Forty-eight hours after transfection, cells were washed once and stimulated with medium or DOTAP alone, 2.5 μg/ml CL075, and ssRNA40 complexed to DOTAP for 3 h. Cells were collected by centrifugation at 1500 rpm for 3 min, and total RNA was extracted using TRIzol reagent (Invitrogen). Knockdown of hTLR8 was confirmed 48 h after siRNA transfection by quantitative PCR using specific primers (Supplemental Table I) and Western blotting with anti–TLR8-N mAb. For knockdown of TLR8 in THP-1 cells, cells were transfected with the Amaxa Cell Line Nucleofector kit V (Lonza) and 30 pmol control or TLR8 siRNA, according to the manufacturer's instructions. Nucleofection was performed twice every 24 h. Forty-eight hours postnucleofection, cells were treated with 10 ng/ml IFN-γ for 15 h and stimulated with the indicated TLR8 ligands. Experiments were repeated three times for confirmation of the results.

Quantitative PCR

Total RNA was extracted using TRIzol reagent and reverse transcribed using the high-capacity cDNA Reverse Transcription kit (Applied Biosystems) and random primers, according to the manufacturer's instructions. Quantitative PCR was performed using the indicated primers (Supplemental Table I) and the StepOne Real-Time PCR System (Applied Biosystems).

Cytokine assay

Monocyte-derived macrophages (5×10^5 /ml) were pretreated with DC1 (20 μM) or DMSO for 4 h and then were stimulated with CL075 (2.5 μg/ml), ssRNA40 complexed to DOTAP (2.5 μg/ml), or LPS (1 μg/ml) or left untreated in the presence of inhibitors for another 24 h. To examine stepwise processing of TLR8-N, monocytes were treated with 10 μM z-FA-FMK in the presence of 20 ng/ml recombinant hGM-CSF for 24 or 48 h and then stimulated with indicated ligands for 24 h. IL-12p40 in culture supernatants was measured by ELISA (R&D Systems).

Flow cytometry

Monocytes and monocyte-derived macrophages that were left untreated or stimulated with 2.5 μg/ml CL075 for 24 h were incubated with FcR Blocking Reagent, human (Miltenyi Biotec) in FACS buffer (PBS containing 5% FCS) for 5 min at 4°C and then incubated with PE mIgG1 or PE anti-human CD80 mAb (1:200) for 30 min at 4°C in the dark. For CD68 staining, cells were fixed and permeabilized by incubating with Fixation/Permeabilization Solution (BD Bioscience) for 20 min at 4°C. Cells were washed twice with 1× BD Perm/Wash buffer and incubated with FITC mIgG2b or FITC anti-human CD68 mAb (1:200) for 30 min at 4°C in the presence of mIgG2b (1:100). After washing twice with FACS buffer (for CD80 staining) or 1× BD Perm/Wash buffer (for CD68 staining), cells were analyzed on a FACSCalibur (BD Bioscience).

Immunoprecipitation

RAW264.7 cells stably expressing hTLR8-FLAG or TLR8Δloop-FLAG cultured in 10-cm dishes were lysed in 1% Nonidet P-40 lysis buffer (50 mM Tris-HCl [pH 7.5], 150 mM NaCl, 10 mM EDTA, 5 mM Na_3VO_4, 30 mM NaF, 2 mM PMSF, and a protease inhibitor mixture) for 10 min at 4°C. Lysates were clarified by centrifugation at 15,000 rpm for 15 min, precleared with protein G–Sepharose (GE Healthcare, Buckinghamshire, U.K.), and incubated with anti-FLAG mAb. The immunoprecipitates were recovered by incubation with protein G–Sepharose for 1 h at 4°C, washed three times with 1% Nonidet P-40 lysis-washing buffer (50 mM Tris-HCl [pH 7.5], 150 mM NaCl, 10 mM EDTA), and resuspended in denaturing buffer. Samples were analyzed by SDS-PAGE (7.5% gel) under reducing conditions, followed by immunoblotting with anti-FLAG pAb and anti–TLR8-N mAb.

Deglycosylation

Monocyte-derived macrophages (5.0×10^5) were lysed in 150 μl lysis buffer. After centrifugation, the supernatants were aliquoted (50 μl each) and incubated with buffer alone, 1 μl Endoglycosidase H (Roche), or 2 μl *N*-glycosidase F (Roche) for 30 min at 37°C. Samples were mixed with denaturing buffer and analyzed by SDS-PAGE under reducing conditions, followed by immunoblotting with anti–TLR8-N mAb.

Pull-down assay

Monocyte-derived macrophages (2.5×10^5 /sample) were lysed in lysis buffer, as described above. After centrifugation at 15,000 rpm for 15 min, supernatants were incubated with 2.5 μg ssRNA, biotinylated ssRNA, or 0.145 μg biotin for 1 h at 4°C. Streptavidin–Sepharose suspended in 1% BSA washing buffer was added to the reaction mixtures and incubated for 1 h at 4°C. After centrifugation, streptavidin beads were washed three times with washing buffer and resuspended in denaturing buffer for 5 min at 95°C. Samples were analyzed by SDS-PAGE under reducing conditions, followed by immunoblotting with anti–TLR8-N mAb.

Confocal microscopy

HEK293 cells (2.0×10^5 cells/well) were plated onto poly-L-lysine–coated micro coverglasses (BD Biosciences) in a 24-well plate. The following day, cells were transfected with the indicated plasmids using FuGENE HD. Twenty-four hours after transfection, cells were washed twice with PBS, fixed with 4% paraformaldehyde for 15 min, and permeabilized with PBS containing 100 μg/ml digitonin and 1% BSA. In the case of human macrophages, fixed cells (2.5×10^4 cells/well) were permeabilized with PBS containing 0.1% Triton X-100 and 2% BSA for 15 min. Fixed cells were blocked in PBS containing 1% BSA and labeled with the indicated primary Abs (2–10 μg/ml) for 60 min at room temperature. Alexa Fluor–conjugated secondary Abs (1:400) were used to visualize the staining of the primary Abs. After mounting with ProLong Gold with DAPI (Molecular Probes), cells were visualized at ×63 magnification with an LSM510 META microscope (Zeiss, Jena, Germany).

Results

Insertion loop between LRR14 and LRR15 is indispensable for hTLR8-mediated signaling

To examine the requirement of proteolytic processing in ligand recognition and signaling by hTLR8, C-terminal FLAG-tagged wild-type TLR8 and truncated mutant forms were provided. TLR8Δloop lacks the insertion loop between LRR14 and LRR15. TLR8-C represents a deletion mutant lacking LRR1–14 and the insertion loop. These were transiently expressed in HEK293 cells and stimulated with a synthetic small molecule (CL075) and ssRNA40 complexed to DOTAP. Wild-type TLR8 was expressed at the expected molecular mass (~150 kDa) and activated NF-κB in response to CL075, but not to ssRNA40, whereas TLR8Δloop failed to respond to both ligands (Fig. 1A, 1B). Cleavage products of TLR8 were undetectable in HEK293 cell lysates in either type of TLR8 expression (Fig. 1B). In addition, TLR8-C did not activate NF-κB in response to CL075 and ssRNA40 (Fig. 1A, 1B).

UNC93B1 physically associates with hTLR8 and regulates intracellular trafficking and signaling of TLR8 (10). When UNC93B1 was coexpressed with wild-type TLR8 in HEK293 cells, CL075-induced TLR8-mediated NF-κB activation was greatly increased concomitantly with the appearance of the N- and C-terminal halves of TLR8, but no response to ssRNA40 was observed (Fig. 1C, 1D). The molecular mass of the C-terminal half of TLR8 was almost the same as that of TLR8-C. In contrast, TLR8Δloop that remained uncleaved could not respond to CL075 or ssRNA40 even though it was coexpressed with UNC93B1 (Fig. 1C, 1D). Again, the

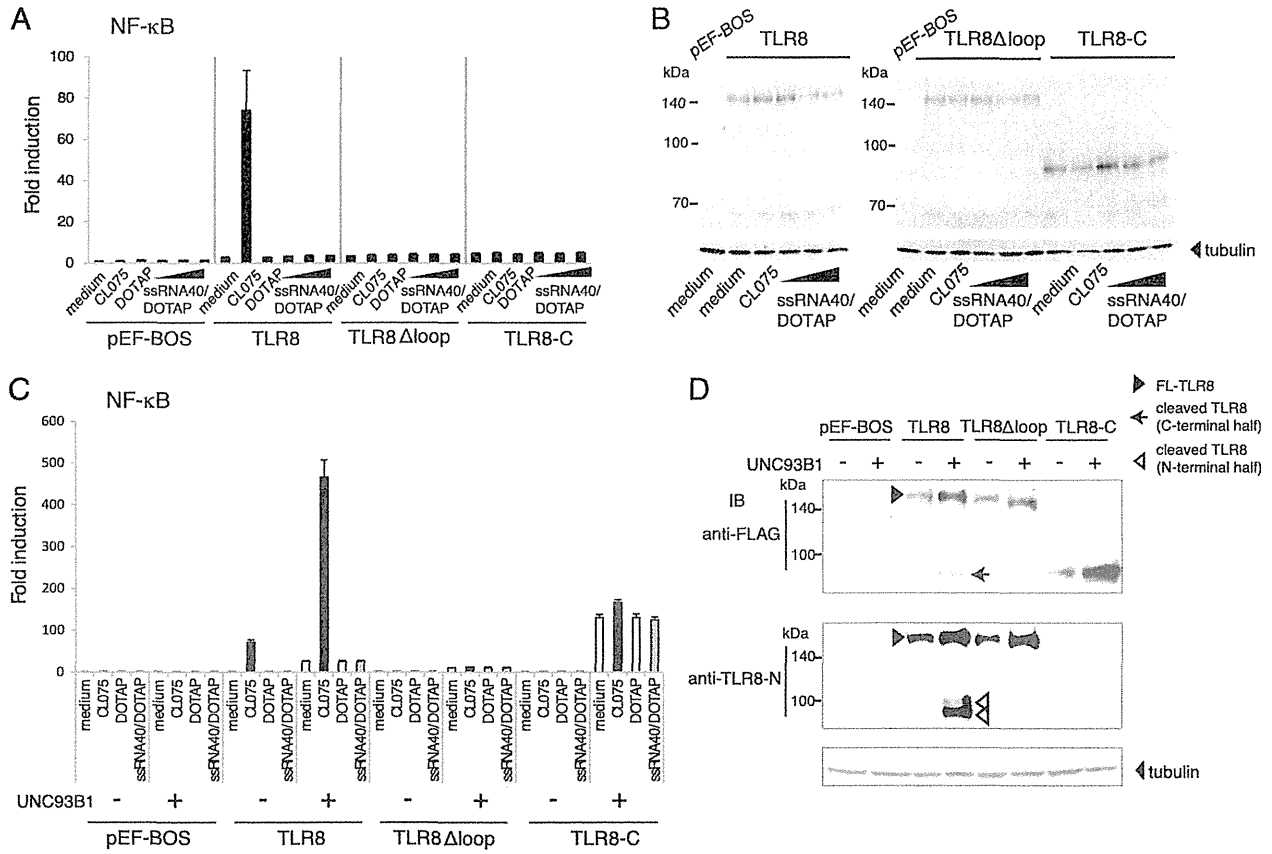

FIGURE 1. The flexible loop between LRR14 and LRR15 was required for CL075-induced TLR8-mediated NF-κB activation in HEK293 cells. (**A**) HEK293 cells were transiently transfected with vector alone or maximum amounts of C-terminal FLAG-tagged wild-type or mutant TLR8 plasmids (TLR8Δloop and TLR8-C), together with NF-κB–luciferase reporter plasmid and phRL-TK. Twenty-four hours after transfection, cells were stimulated with CL075 (2.5 μg/ml), DOTAP alone, or ssRNA40 complexed with DOTAP (2.5, 5, or 10 μg/ml) or were left untreated. Luciferase activity was measured 12 h after stimulation and expressed as fold induction relative to the activity of unstimulated cells. Representative data from three independent experiments, each performed in triplicate, are shown (mean ± SD). (**B**) Protein expression of wild-type and mutant TLR8 in HEK293 cells. Cell lysates prepared in (A) were subjected to SDS-PAGE (7.5%), followed by Western blotting with anti-FLAG mAb and anti–tubulin-α mAb. (**C**) Coexpression of UNC93B1 promoted CL075-induced TLR8-mediated NF-κB activation in HEK293 cells. HEK293 cells were transfected with the indicated plasmids together with NF-κB–luciferase reporter plasmid and phRL-TK. Cells were stimulated with 2.5 μg/ml CL075, DOTAP alone, or ssRNA40 complexed to DOTAP or were left untreated. Luciferase activity was measured 12 h after stimulation and expressed as fold induction relative to the activity of unstimulated cells. (**D**) Cell lysates prepared in (C) were subjected to SDS-PAGE (7.5%), followed by Western blotting with anti-FLAG mAb, anti–TLR8-N mAb, and anti–tubulin-α mAb. Filled arrowheads indicate full-length TLR8. Open arrowheads indicate N-terminal half of TLR8. Arrow indicates C-terminal half of TLR8.

truncated C-terminal half of TLR8 was unable to act as an RNA-sensing receptor. These results suggest that the loop region between LRR14 and LRR15 is crucial for ligand-induced TLR8-mediated signaling, as well as proteolytic processing of TLR8. UNC93B1 promoted proteolytic cleavage of TLR8 by facilitating ER exit of TLR8. In HEK293 cells transiently expressing TLR8, small amounts of cleaved TLR8 molecules appear to participate in the recognition of CL075 (Fig. 1A). Although the reason why ssRNA40 could not activate TLR8 in HEK293 cells ectopically expressing UNC93B1 is unclear, one possible interpretation is that oligomerization of multiple TLR8 molecules is required for ssRNA40-induced NF-κB activation. Notably, overexpressed wild-type and mutant TLR8, especially TLR8-C, activate NF-κB in a ligand-independent manner only when coexpressed with UNC93B1 (Fig. 1C, Supplemental Fig. 1), suggesting that transient overexpression and trafficking may allow TLR8–TIR domains to access each other, leading to activation of downstream signaling.

Cleavage of endogenous TLR8 in IFN-γ–treated THP-1 cells

THP-1 cells expressed TLR8 mRNA, which was upregulated by stimulation with IFN-γ (Fig. 2A) (40). To examine the structure of endogenous TLR8, we generated a pAb that recognizes the hTLR8 C-terminal peptides. The anti–TLR8-C pAb specifically recognized the full-length and C-terminal half of TLR8 but not N-terminal half of TLR8, hTLR7, or hTLR9 (Supplemental Fig. 2). In the IFN-γ–treated THP-1 cells, both full-length and C-terminal half of TLR8 proteins were detected by Western blotting with anti–TLR8-C Ab, indicating that endogenous TLR8 undergoes proteolytic processing (Fig. 2B). IFN-γ–treated THP-1 cells induced IL-12p40 mRNA expression in response to CL075, as well as ssRNA40, which was abolished by TLR8 knockdown (Fig. 2C).

Cleaved form of TLR8 is predominant in human primary monocytes and monocyte-derived macrophages

We investigated structural features of endogenous TLR8 in human primary cells, including monocytes and monocyte-derived macrophages. $CD14^+$ monocytes were successfully differentiated into macrophages after GM-CSF treatment for 6 d, in which the macrophage marker CD68 was greatly induced and the costimulatory molecule CD80 was upregulated by stimulation with CL075 (Supplemental Fig. 3). Immunoblotting with anti–TLR8-N and anti–TLR8-C Abs under reducing or nonreducing conditions clearly showed that TLR8 underwent proteolytic processing, and cleaved forms of TLR8 were predominant in monocytes and monocyte-derived macrophages (Fig. 3A). The TLR8 N-terminal halves consisted of two bands with a molecular mass ~100 and ~90 kDa. The C-terminal half was detected as a single band with a molecular mass ~90 kDa (Fig. 3A). None of the bands corresponding to TLR8 was observed in B cells, confirming the specificity of the TLR8 Abs used.

Upon stimulation with CL075 or ssRNA40 complexed to DOTAP, monocyte-derived macrophages produced a high level of IL-12p40 and some IL-6 and TNF-α, but their expression varied among different donors/individuals (Fig. 3B). Human monocyte-derived macrophages expressed low levels of TLR7; therefore, we examined whether the response to CL075 and ssRNA40 depended on TLR8 by knockdown analysis in macrophages. CL075- and ssRNA40-induced IL-12p40 mRNA expression was significantly reduced when TLR8 expression was knocked down at both the mRNA and protein levels (Fig. 3C). Notably, the expression and processing of TLR8 were mostly unaltered during differentiation from $CD14^+$ monocytes to macrophages, with the exception of day-1 monocytes after GM-CSF treatment: full-length TLR8 disappeared, and the lower band of TLR8-N was detected primarily (Fig. 4A). The response of TLR8 to ssRNA40 was unchanged during differentiation (Fig. 4B). Absence of full-length TLR8 at day 1 upon differentiation of monocytes with GM-CSF was observed consistently, irrelevant of the donor. These results suggest that the cleaved form of TLR8 is a functional receptor in human primary cells.

Both furin-like proprotein convertase and cathepsins are involved in stepwise processing of hTLR8

Two TLR8-Ns with different molecular masses were detected in monocyte and macrophage lysates; thus, we examined the proteases involved in TLR8 cleavage in human primary cells using protease inhibitors. Treatment of macrophages with z-FA-FMK, a cysteine protease inhibitor that blocks cathepsin proteolytic activity, failed to reduce both TLR8 cleavage and response to TLR8 agonists, probably because the cleaved form of TLR8 was abundant in macrophages (data not shown). When monocytes were differentiated into macrophages with GM-CSF in the presence of z-FA-FMK, an ~100-kDa upper band of TLR8-N accumulated from days 1 to 3, compared with DMSO-treated monocyte differentiation that mainly contained the lower band of TLR8-N (Fig. 5A, *upper panels*). This suggests that the upper band of TLR8-N is

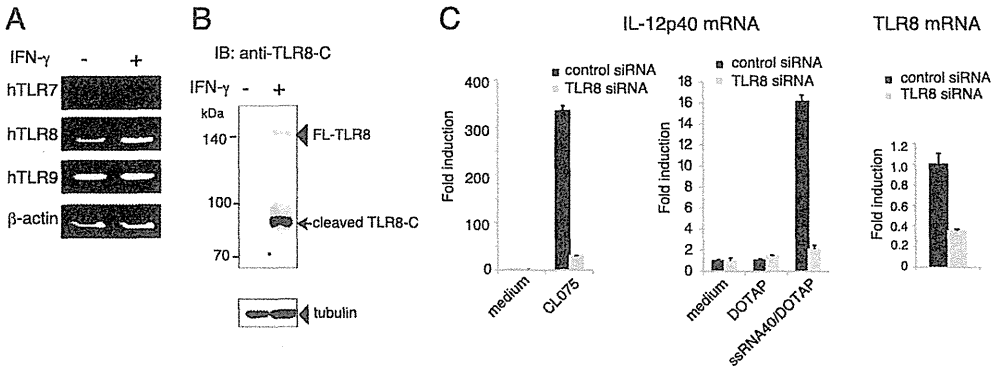

FIGURE 2. Human TLR8 underwent proteolytic processing in IFN-γ–treated THP-1 cells. **(A)** THP-1 cells (5×10^5/ml) were stimulated with 20 ng/ml IFN-γ or were left untreated for 15 h. Expression of TLR7, TLR8, and TLR9 mRNAs was analyzed by RT-PCR using specific primers (Supplemental Table I) (56). **(B)** Lysates of IFN-γ–treated or untreated THP-1 cells were subjected to SDS-PAGE, followed by Western blotting with anti–hTLR8-C pAb and anti–tubulin-α mAb. Arrowhead indicates full-length TLR8. Arrow indicates C-terminal half of TLR8. **(C)** Control or TLR8–knocked down IFN-γ–treated THP-1 cells (5×10^5/ml) were stimulated with medium alone, 2.5 μg/ml CL075, DOTAP alone, or 2.5 μg/ml ssRNA40 complexed to DOTAP. After 12 h, total RNA was extracted, and quantitative PCR was performed using primers for the IL-12p40 and TLR8 genes. Expression of genes was normalized to β-actin mRNA expression. Knockdown efficiency is shown (*right panel*). Representative data from two independent experiments are shown (mean ± SD).

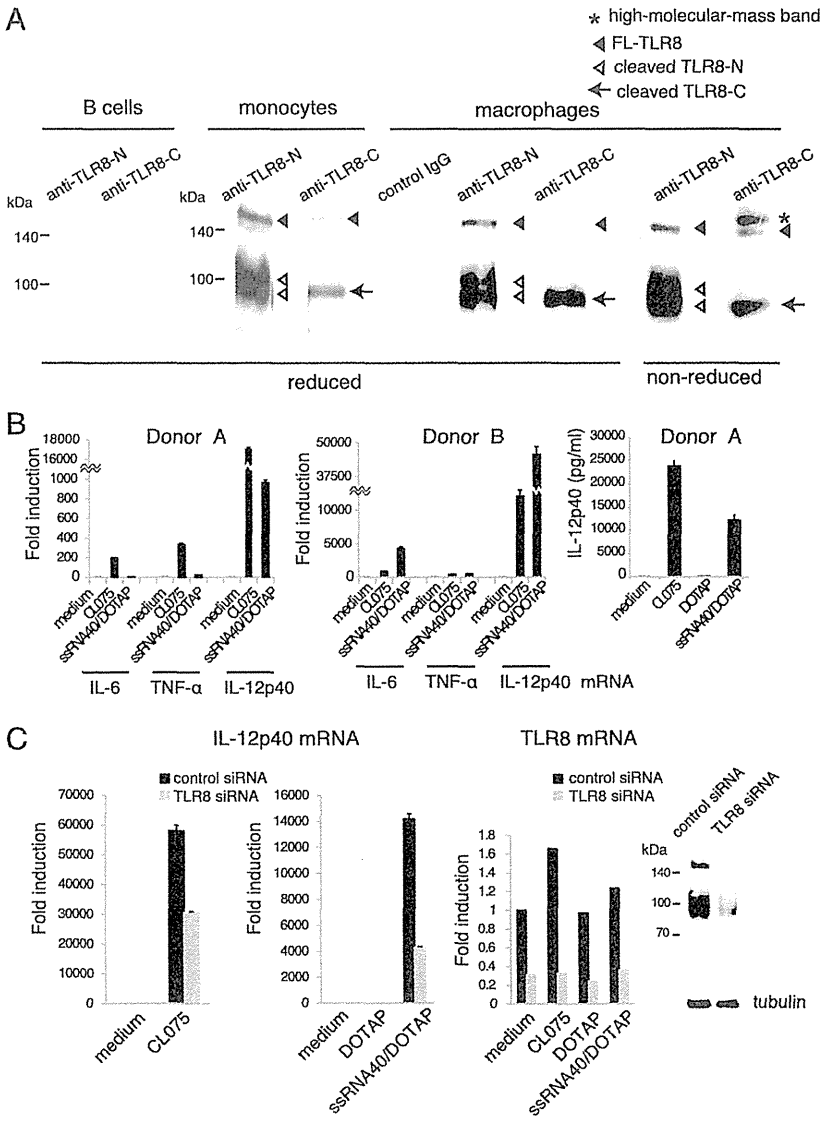

FIGURE 3. Cleaved form of TLR8 was predominant in human monocytes and monocyte-derived macrophages. (**A**) Lysates of human monocytes and monocyte-derived macrophages were subjected to SDS-PAGE under reducing or nonreducing conditions, followed by Western blotting with anti–TLR8-N mAb, anti–TLR8-C pAb, or control rabbit IgG. Lysates of B cells were used as cellular negative control. Filled arrowheads indicate full-length TLR8 (~150 kDa). Open arrowheads indicates N-terminal halves of TLR8 (~100 and ~90 kDa). Arrows indicate C-terminal half of TLR8 (90 kDa). Asterisk indicates high molecular mass band of TLR8. (**B**) Human monocyte-derived macrophages from different healthy donors were stimulated with the indicated ligands for 3 h, and IL-6, IL-12p40, and TNF-α transcripts were measured by quantitative PCR (*left* and *middle panels*). Protein levels of IL-12p40 in culture supernatants after 24 h of stimulation (donor A) were quantified using ELISA (*right panel*). (**C**) TLR8 is indispensable for ssRNA-induced cytokine production by human macrophages. Monocyte-derived macrophages (5×10^5/ml) were transfected with 30 pmol control or TLR8 siRNA. Forty-eight hours after transfection, cells were washed and stimulated with medium alone, 2.5 μg/ml CL075, DOTAP alone, or 2.5 μg/ml ssRNA40 complexed to DOTAP for 3 h, and IL-12p40 mRNA was measured by quantitative PCR. Knockdown of TLR8 mRNA and protein was confirmed by quantitative PCR and Western blotting with anti–TLR8-N mAb, respectively. Representative data from three independent experiments are shown (mean ± SD).

a premature form, and cysteine proteases, such as the cathepsin family, participate in further processing to generate the mature form of TLR8-N. Correlatively, when day-1 and day-2 monocytes were stimulated with CL075 or ssRNA40 complexed to DOTAP for 24 h, IL-12p40 production was decreased in z-FA-FMK–treated monocytes compared with DMSO-treated cells (Fig. 5A, *lower panel*). Considering that TLR7 was barely expressed in day- 1 to day-3 differentiated monocytes, involvement of TLR7 in CL075-induced IL-12p40 production is minimal, at best, under these experimental conditions. LPS-induced IL-12p40 production by these differentiated monocytes was unaltered in the presence of z-FA-FMK (data not shown).

A recent study demonstrated that furin-like proprotein convertase participates in processing of hTLR7 (30). We assessed the role of furin-like proprotein convertase in hTLR8 processing. Inhibition of furin-like proprotein convertase using DC1 reduced the response of macrophage TLR8 to CL075 and ssRNA40 but not to LPS (Fig. 5B). The cleaved TLR8-C and two TLR8-Ns, especially the upper band of TLR8-N, were reduced in DC1-treated macrophages compared with DMSO-treated cells (Fig. 5B, data not shown). Because a potential furin-like proprotein convertase–recognition site is present in the flexible loop between LRR14 and LRR15 of hTLR8, we made TLR8 mutant R467A/R470A/R472A/R473A in which the arginine residues in the potential furin-like proprotein convertase–recognition site in the flexible loop were substituted with alanine. This TLR8 mutant completely failed to undergo proteolytic processing when ectopically expressed in HEK293 cells, with or without UNC93B1, resulting in no activation of NF-κB in response to CL075 (Fig. 5C). These results indicate that furin-like proprotein convertase is indispensable for TLR8 cleavage at an initial step. Thus, both furin-like proprotein convertase and cathepsins are involved in stepwise processing of TLR8-N in human primary monocytes and macrophages.

N- and C-terminal halves of hTLR8 associate with each other and ssRNA40 binds to the cleaved/associated TLR8

To explore the association of the N- and C- terminal halves of TLR8, C-terminal FLAG-tagged wild-type and mutant hTLR8 were stably expressed in the mouse macrophage cell line RAW264.7. Wild-type TLR8, but not TLR8Δloop, underwent proteolytic processing in RAW cells, similar to an endogenous TLR8 in human macrophages (Fig. 6A). The N-terminal half of TLR8 coimmunoprecipitated with the C-terminal half of TLR8 under reducing and nonreducing conditions, suggesting that both the N- and

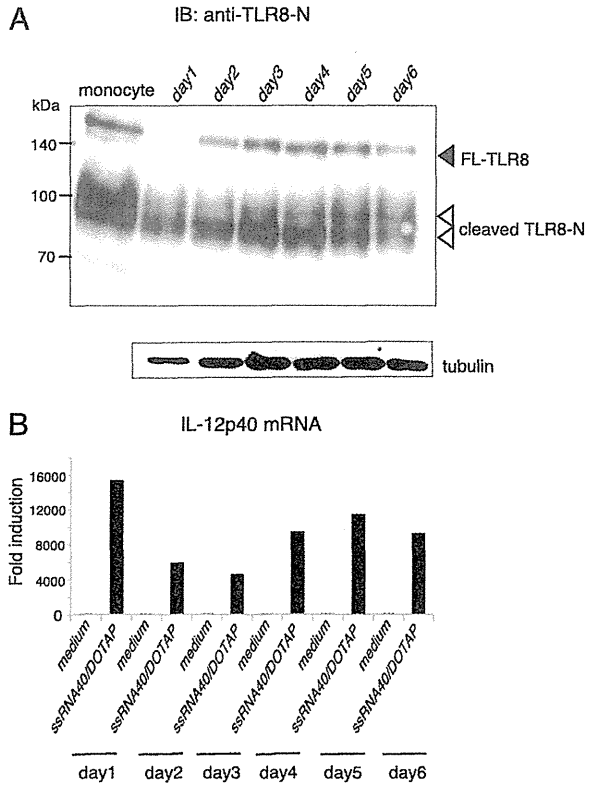

FIGURE 4. Expression and proteolytic processing of hTLR8 during differentiation from monocytes to macrophages. **(A)** $CD14^+$ human monocytes were cultured in medium containing GM-CSF for 1–6 d. TLR8 protein in differentiating cells was analyzed by western blotting with anti–TLR8-N mAb. Filled arrowhead indicates full-length TLR8. Open arrowheads indicate cleaved N-terminal halves of TLR8. **(B)** Response to ssRNA40 during differentiation from monocytes to macrophages. Differentiating cells were stimulated with 2.5 μg/ml ssRNA40 complexed to DOTAP for 3 h, and IL-12p40 transcript was measured by quantitative PCR. Representative data from more than three independent experiments are shown. In every experiment, full-length TLR8 was absent at day 1 upon differentiation of monocytes to macrophages after GM-CSF treatment.

C-terminal halves were noncovalently associated with each other in macrophages (Fig. 6B). We examined the interaction of ssRNA with TLR8 by pull-down assay using human macrophage lysates and biotinylated ssRNA40. After incubation of biotinylated ssRNA40 in the human macrophage lysates, ssRNA40–receptor complex was pulled down with avidin-Sepharose. Both the N- and C-terminal halves of TLR8 were pulled down, indicating that ssRNA40 bound to the cleaved/associated form of TLR8 (Fig. 6C).

Intracellular trafficking of hTLR8

TLR8 localizes to the ER and early endosome in primary human monocytes and HeLa cells transiently expressing hTLR8 (10). We examined the glycosylation of TLR8 protein in monocyte-derived macrophages with Endoglycosidase H, which hydrolyzes the high-mannose type *N*-glycans and *N*-glycosidase F that cleaves all types of asparagine-bound *N*-glycans. Deglycosylation analysis clearly showed that TLR8 was cleaved after passing through the Golgi, because most of the sugars on the cleaved TLR8-N were resistant to Endoglycosidase H and sensitive to *N*-glycosidase F (Fig. 7A). In contrast, N-linked sugars on full-length TLR8 were sensitive to Endoglycosidase H, indicating that an ~150-kDa band corresponding to full-length TLR8 was derived from the ER (Fig. 7A). The full-length TLR8 proteins accumulated in macrophages by brefeldin A treatment that disrupted the Golgi pathway (Fig. 7B).

Coexpression of UNC93B1 with TLR8 facilitated intracellular trafficking of TLR8 in HEK293 cells, resulting in accumulation of cleaved TLR8 (Fig. 1D). Confocal immunofluorescence analysis demonstrated that colocalization of TLR8 with p115 (Golgi-resident protein) was increased by UNC93B1 coexpression (Fig. 8A). TLR8 colocalized with MPR (late endosome marker protein), but not LysoTracker (lysosome marker), in UNC93B1-expressing cells (Fig. 8A). In human monocyte-derived macrophages, TLR8 colocalized with early endosome Ag 1 (early endosome marker protein), MPR, and calnexin (ER protein) but not with Lamp-1 (lysosome marker protein) (Fig. 8B). Taken together, these results indicated that TLR8 exits the ER, passes through the Golgi, and is targeted to early/late endosomes where the processing occurs.

Discussion

In the current study, we showed for the first time, to our knowledge, that proteolytic processing of TLR8 occurs in human primary cells, including monocytes and monocyte-derived macrophages, in a different manner from that of TLR7 and TLR9 cleavage. The insertion loop between LRR14 and LRR15 in TLR8 ECD is indispensable for cleavage and stepwise processing that occurs in the N-terminal fragment. Both furin-like proprotein convertase and cathepsins contribute to TLR8 cleavage in the early/late endosomes. Recent structural analysis of hTLR8 ECD–chemical ligand complex demonstrated that purified TLR8 ECD protein is cleaved at the loop region, and the N- and C-terminal halves remain associated, which contributes to ligand recognition and dimerization (39). Indeed, noncovalent association of the N-terminal half of TLR8 with the C-terminal half was detected by immunoprecipitation assay in RAW macrophages stably expressing hTLR8 (Fig. 6B). Furthermore, a pull-down assay revealed that ssRNA bound to the cleaved/associated form of TLR8 in human macrophages (Fig. 6C).

TLR8 belongs to the same subfamily as TLR7 and TLR9 (14, 15), but localization and signaling are quite different. We showed that hTLR8 localized to the ER and the early/late endosomes, but not to the lysosome, in monocytes and macrophages (Fig. 8B) (10), whereas mTLR7 and mTLR9 localized to the endolysosomes of macrophages and pDCs (8). The pH-dependent cathepsin family and AEP are involved in the stepwise processing of TLR7 and TLR9 at the C-terminal portion in mouse macrophages and DCs, although their contribution depends on cell type (24–29). In contrast, hTLR7 is processed at neutral pH, which is mediated with furin-like proprotein convertase (30). In the case of hTLR8, cathepsins mediate second-step processing of the N-terminal half, resulting in the generation of the mature form of the N-terminal half (Fig. 5A). Like hTLR7 processing, furin-like proprotein convertase is indispensable for TLR8 cleavage at an early step (Fig. 5B, 5C). Indeed, potential furin-like proprotein convertase–recognition sites are present in LRR14 and the flexible loop of hTLR8; one such site is located just before the N-terminus of the C-terminal ECD fragment (39). The TLR8 mutant R467A/R470A/R472A/R473A, in which arginine residues in the potential furin-like proprotein convertase–recognition site were substituted with alanine, was uncleaved when ectopically expressed in HEK293 cells and failed to transmit signals upon stimulation with CL075 (Fig. 5C). Although a putative asparagine cleavage site for AEP is found in the flexible loop of hTLR8 compared with that of mTLR7/9 (27), this site is located within the TLR8-C sequence, suggesting that AEP does not participate in TLR8 cleavage. Thus, proteases involved in processing of TLR7, TLR8, and TLR9 appear to be different and might depend on the localization of receptors and species- and cell type–specific protease distribution.

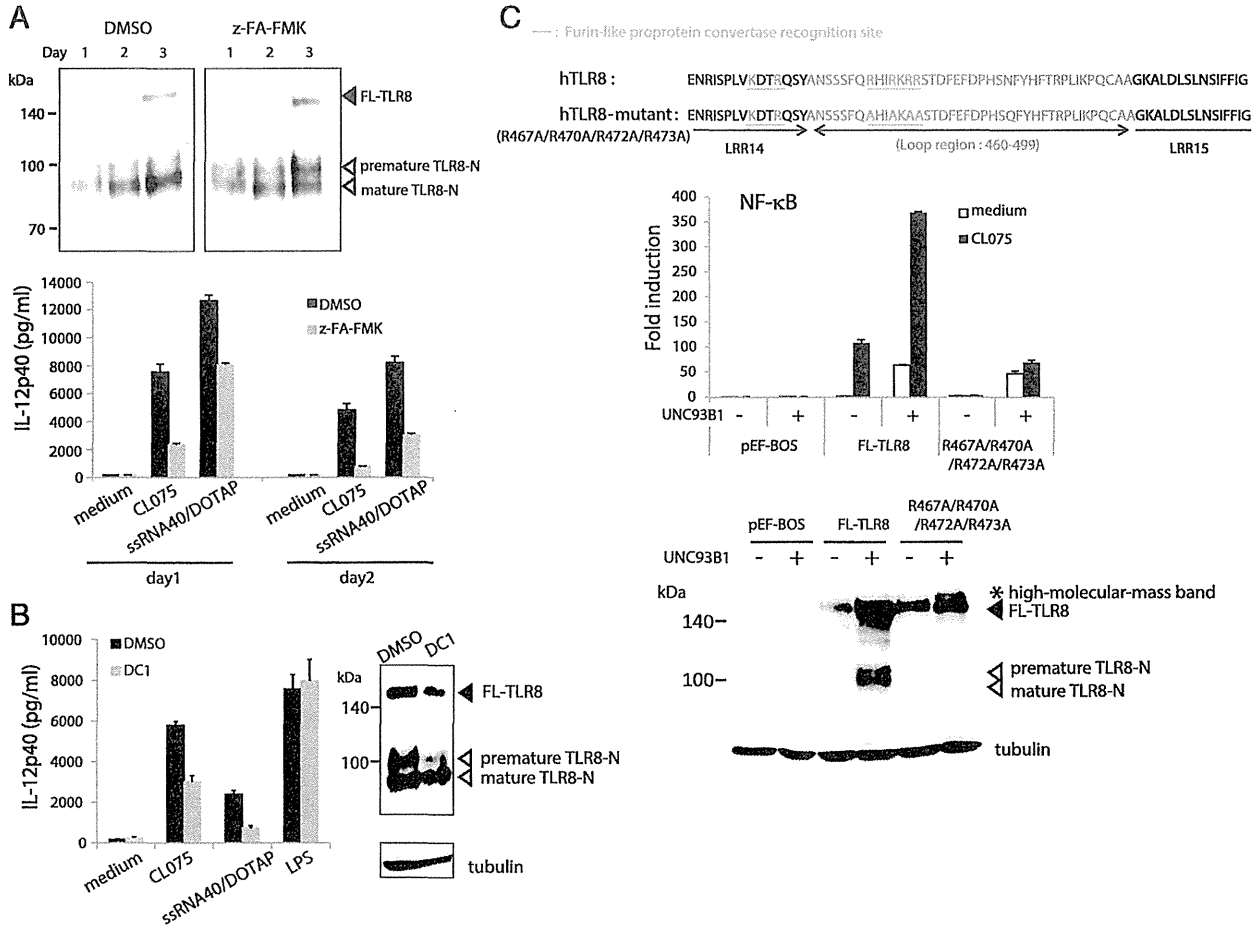

FIGURE 5. Furin-like proprotein convertases and cathepsins are involved in stepwise processing of hTLR8. (**A**) Monocytes were treated with GM-CSF in the presence or absence of 10 μM z-FA-FMK for up to 3 d. At day 1, day 2, and day 3, cells were lysed, and lysates were subjected to SDS-PAGE under reducing conditions, followed by Western blotting with anti–TLR8-N mAb (*upper panels*). The day-1 and day-2 monocytes were stimulated with medium alone, CL075 (2.5 μg/ml), or ssRNA40 complexed to DOTAP (2.5 μg/ml) for 24 h. IL-12p40 in the culture supernatants was measured using ELISA (*lower panel*). (**B**) Monocyte-derived macrophages were pretreated with 20 μM DC1 for 4 h and then stimulated with medium alone, CL075 (2.5 μg/ml), ssRNA40 complexed to DOTAP (2.5 μg/ml), or LPS (1 μg/ml) for 24 h. IL-12p40 in the culture supernatants was measured using ELISA (*left panel*). Lysates of DC1-treated macrophages were analyzed by Western blotting with anti–TLR8-N mAb and anti–tubulin-α mAb (*right panel*). (**C**) The potential furin-like proprotein convertase–recognition sites in LRR14 and insertion loop of hTLR8 (*upper panel*). Furin-like proprotein covertase–recognition site is R/K-Xn-R/K (X, any amino acid residue; n = 0, 2, 4, or 6). HEK293 cells were transfected with empty vector, wild-type TLR8 or R467A/R470A/R472A/R473A TLR8 mutant plasmid together with NF-κB–luciferase reporter plasmid and phRL-TK (*middle panel*). Cells were stimulated with 2.5 μg/ml CL075 or were left untreated. Luciferase activity was measured 12 h after stimulation and expressed as fold induction relative to the activity of unstimulated cells (mean ± SD). Cell lysates prepared in the reporter assay (medium stimulation) were subjected to SDS-PAGE (7.5%), followed by Western blotting with anti–TLR8-N mAb and anti–tubulin-α mAb (*bottom panel*). Closed arrowhead indicates full-length TLR8. Open arrowheads indicate premature and mature TLR8-N. Asterisk indicates high molecular mass band of TLR8. Representative data from two independent experiments are shown.

In freshly isolated human monocytes, cathepsins B and L are distributed in endosomes rather than lysosomes, and their sp. act. is observed in endosomal, but not in lysosomal, fractions (41). In addition, both cathepsins are expressed in HEK293 and THP-1 cells, whereas cathepsin S is expressed in THP-1 cells but not in HEK293 cells (K. Iwano, A. Watanabe, and M. Matsumoto, unpublished data). Considering the endosomal, but not lysosomal, localization of hTLR8, stepwise processing of hTLR8 by furin-like proprotein convertase and members of the cathepsin family, such as cathepsins B and L, might occur in early/late endosomes.

UNC93B1 mediates ER exit of TLR8, resulting in the accumulation of cleaved TLR8 in HEK293 cells (Fig. 1D). Notably, the TLR8-activating ability was different between CL075 and ssRNA40 in HEK293 cells transiently expressing TLR8 (Fig. 1). Structural analysis of unliganded and liganded TLR8 ECD revealed that cleaved/associated TLR8 dimerizes without ligand, and ligand binding to both N- and C-terminal halves induces structural reorganization of the TLR8 dimer (39). Mutagenesis analysis showed that interaction sites of TLR8 ECD with ssRNA appear to differ from those with chemical ligands. Oligomerization of TLR8 dimer might be required for ssRNA-induced signaling like dsRNA-induced TLR3-mediated signaling (42). In HEK293 cells, a small number of cleaved/associated TLR8 molecules is unable to induce signals to activate NF-κB in response to ssRNA40. In any case, our cellular analysis indicates that cleaved/associated TLR8 is responsible for recognition of both chemical ligands and ssRNA, and it induces innate immune responses in human primary cells.

Recent reports showed that dsRNA-sensing TLR3 undergoes cathepsin-mediated cleavage in a cell type–dependent manner (43–45). In addition, TLR3 recognizes incomplete stem structures formed in ssRNA (46). The nucleic acid–sensing TLRs respond to

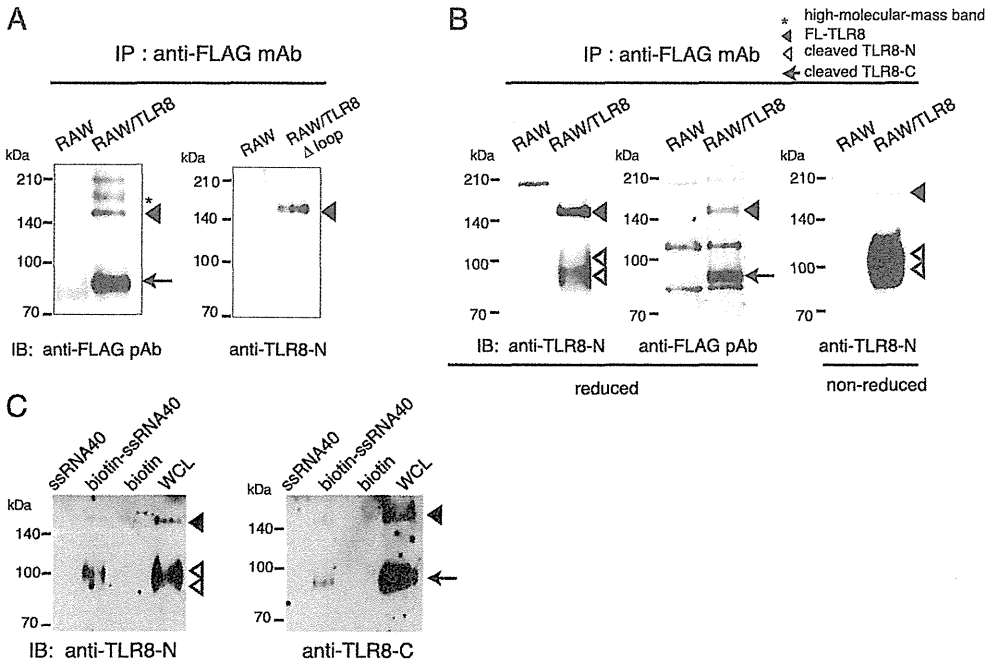

FIGURE 6. The N-terminal half of TLR8 is noncovalently associated with the C-terminal half. (**A**) Immunoblot analysis of RAW264.7 cells stably expressing C-terminal FLAG-tagged hTLR8 or hTLR8Δloop mutant. Cell lysates were immunoprecipitated (IP) with anti-FLAG mAb. The immunoprecipitates were resolved by SDS-PAGE, followed by immunoblotting (IB) with anti-FLAG pAb or anti–TLR8-N mAb. (**B**) Cell lysates of RAW264.7 cells stably expressing C-terminal FLAG-tagged hTLR8 were immunoprecipitated with anti-FLAG mAb. The immunoprecipitates were resolved by SDS-PAGE under reducing and nonreducing conditions, followed by immunoblotting with anti–TLR8-N mAb. The blot was reprobed with anti-FLAG pAb (*middle panel*). The ~210-kDa band is a nonspecific band observed in RAW cells. (**C**) ssRNA40 bound to the cleaved TLR8. Lysates of human macrophages were incubated with ssRNA40 (2.5 μg), biotinylated ssRNA40 (2.5 μg), or biotin (0.145 μg) or were left untreated for 1 h at 4°C and pulled down with streptavidin-Sepharose. Samples were analyzed by SDS-PAGE under reducing conditions, followed by immunoblotting with anti–TLR8-N mAb and anti–TLR8-C pAb.

microbial nucleic acid, as well as to endogenous self nucleic acids, in a sequence-independent, but motif-dependent, manner. Hence, the cleaved/associated form of receptors might be beneficial for recognition of nucleic acids with different nucleotide sequences and structures (47).

The role of TLR8 in antiviral immunity in humans remains unknown. In the case of HIV infection, TLR8 signaling appears to benefit HIV replication (48), but another study demonstrated an anti-HIV function for TLR8 (49). TLR8 expressed in neutrophils mediates neutrophil extracellular trap formation in HIV-1 infection via recognition of viral nucleic acids, which is useful for HIV-1 elimination (50). In addition, TLR8-mediated IL-12p70 production by monocytes polarizes naive $CD4^+$ T cells into Th1 cells that mediate cellular immunity (51). Thus, TLR8 triggers important antimicrobial signals in distinctive cells that express TLR8 but not other nucleic acid–sensing TLRs.

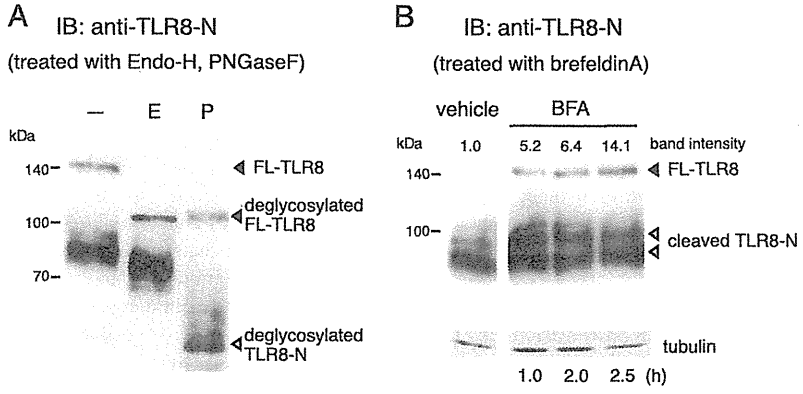

FIGURE 7. Cleaved TLR8 was generated after traveling through the Golgi. (**A**) Immunoblot (IB) analysis of monocyte-derived macrophage lysates (5×10^5) incubated with 1 μl Endoglycosidase H (E) or 2 μl *N*-glycosidase F (P) for 30 min at 37°C. Anti–TLR8-N mAb was used to detect full-length and cleaved TLR8. (**B**) Accumulation of full-length TLR8 by treatment of human macrophages with brefeldin A. Human macrophages were treated with brefeldin A (2 μg/ml), a reagent that disrupts the Golgi, or vehicle for the indicated lengths of time. Cell lysates were separated by SDS-PAGE under reducing conditions, followed by immunoblotting with anti–TLR8-N mAb. The band intensity of FL-TLR8 was quantified using National Institutes of Health ImageJ software and normalized to that of tubulin. Results are expressed as fold intensity relative to the intensity of vehicle-treated cells.

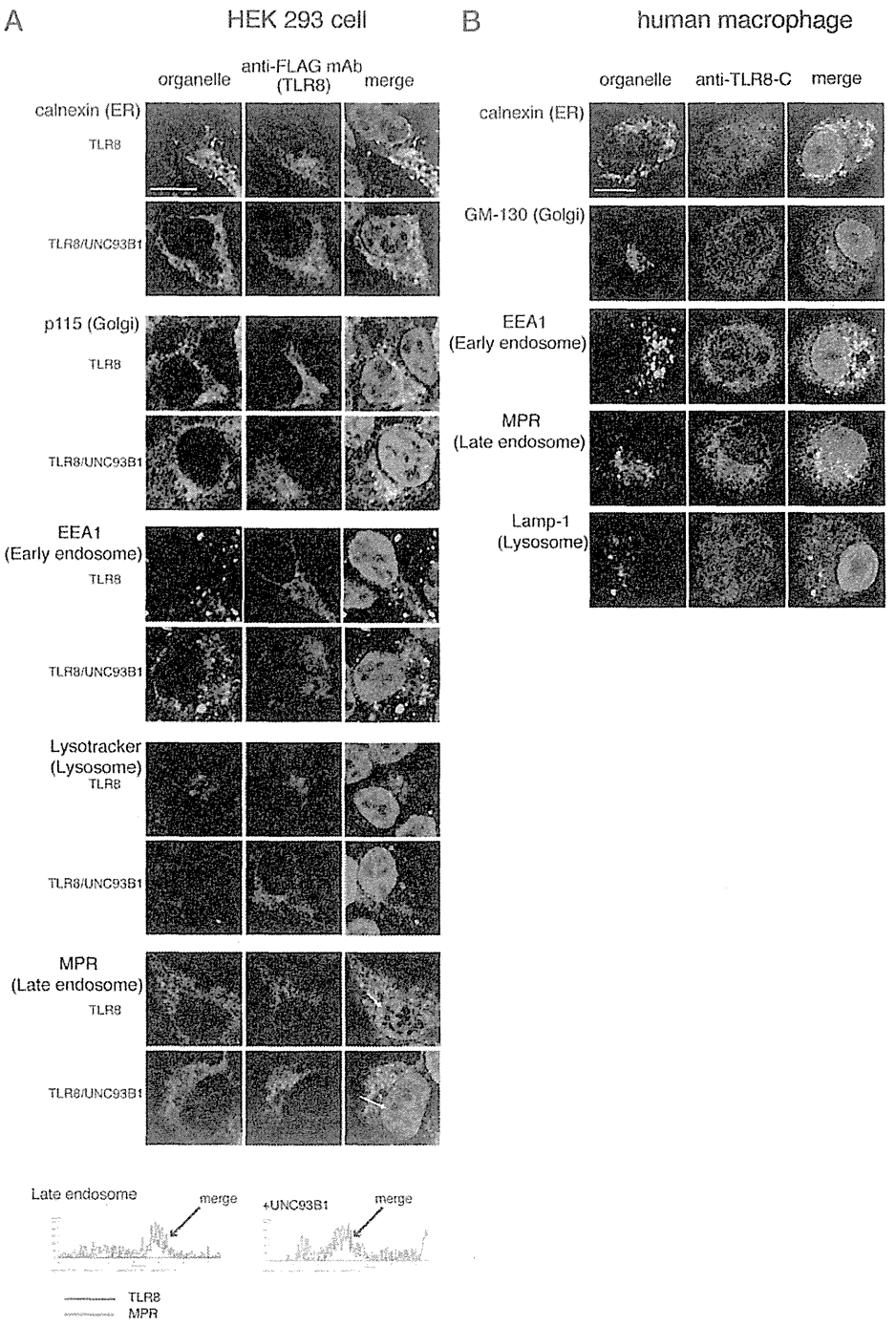

FIGURE 8. TLR8 localized to the early/late endosomes in human macrophages. (**A**) UNC93B1 facilitated intracellular trafficking of TLR8. HEK293 cells expressing FLAG-tagged hTLR8, with or without UNC93B1, were fixed, permeabilized, and stained with anti-FLAG mAb and the indicated pAbs against organelle marker proteins, followed by Alexa Fluor 488–labeled or Alexa Fluor 568–labeled secondary Ab. Red, organelle markers; green, TLR8; blue, DAPI-stained nuclei. Scale bar, 10 μm. Graphs display the measured fluorescence intensity along the white line in the merged panels of MPR and TLR8 with or without UNC93B1. (**B**) Subcellular localization of endogenous TLR8 in monocyte-derived macrophages. Macrophages were fixed, permeabilized, and stained with anti–TLR8-C pAb and the indicated mouse mAbs against organelle marker proteins, followed by Alexa Fluor 488–labeled or Alexa Fluor 568–labeled secondary Ab. Red, organelle markers; green, TLR8; blue, DAPI-stained nuclei. Scale bar, 10 μm.

TLR7 and TLR9 are closely associated with autoimmune disorders because of their expression in B cells and pDCs (52, 53). The relationship between TLR8 and autoimmune disorders was suggested in a TLR8-knockout mouse study that showed a pivotal role for mTLR8 in the regulation of TLR7 expression and prevention of spontaneous autoimmunity (54). In addition, a recent study using hTLR8-transgenic mice clearly demonstrated the connection between TLR8 and autoimmune inflammation (55). TLR8 was shown to induce proinflammatory cytokine production in response to microRNA within exosomes from tumor cells (38). In view of the unique expression profile and signaling skewed toward NF-κB activation, TLR8 might be involved in the development of inflammatory disorders in a distinct manner. Identification of endogenous and exogenous TLR8 ligands and their recognition mechanisms are important for a full understanding of the role of TLR8 in innate immunity and protection against undesirable inflammation and autoimmune responses.

Acknowledgments

We thank our laboratory members for valuable discussions. We also thank M. Nakai, R. Takemura, K. Mugikura, Y. Takeda, A. Maruyama, and K. Takashima for preparing blood cells. We also thank Dr. K. Miyake, Dr. S. Akira, and Dr. S. Nagata for providing the plasmids.

Disclosures

The authors have no financial conflicts of interest.

References

1. Medzhitov, R., and C. A. Janeway, Jr. 1997. Innate immunity: the virtues of a nonclonal system of recognition. *Cell* 91: 295–298.
2. Akira, S., S. Uematsu, and O. Takeuchi. 2006. Pathogen recognition and innate immunity. *Cell* 124: 783–801.
3. Barton, G. M., and J. C. Kagan. 2009. A cell biological view of Toll-like receptor function: regulation through compartmentalization. *Nat. Rev. Immunol.* 9: 535–542.
4. Matsumoto, M., K. Funami, M. Tanabe, H. Oshiumi, M. Shingai, Y. Seto, A. Yamamoto, and T. Seya. 2003. Subcellular localization of Toll-like receptor 3 in human dendritic cells. *J. Immunol.* 171: 3154–3162.
5. Latz, E., A. Schoenemeyer, A. Visintin, K. A. Fitzgerald, B. G. Monks, C. F. Knetter, E. Lien, N. J. Nilsen, T. Espevik, and D. T. Golenbock. 2004. TLR9 signals after translocating from the ER to CpG DNA in the lysosome. *Nat. Immunol.* 5: 190–198.
6. Tabeta, K., K. Hoebe, E. M. Janssen, X. Du, P. Georgel, K. Crozat, S. Mudd, N. Mann, S. Sovath, J. Goode, et al. 2006. The Unc93b1 mutation 3d disrupts exogenous antigen presentation and signaling via Toll-like receptors 3, 7 and 9. *Nat. Immunol.* 7: 156–164.
7. Brinkmann, M. M., E. Spooner, K. Hoebe, B. Beutler, H. L. Ploegh, and Y. M. Kim. 2007. The interaction between the ER membrane protein UNC93B and TLR3, 7, and 9 is crucial for TLR signaling. *J. Cell Biol.* 177: 265–275.
8. Kim, Y. M., M. M. Brinkmann, M. E. Paquet, and H. L. Ploegh. 2008. UNC93B1 delivers nucleotide-sensing toll-like receptors to endolysosomes. *Nature* 452: 234–238.
9. Fukui, R., S. Saitoh, F. Matsumoto, H. Kozuka-Hata, M. Oyama, K. Tabeta, B. Beutler, and K. Miyake. 2009. Unc93B1 biases Toll-like receptor responses to nucleic acid in dendritic cells toward DNA- but against RNA-sensing. *J. Exp. Med.* 206: 1339–1350.
10. Itoh, H., M. Tatematsu, A. Watanabe, K. Iwano, K. Funami, T. Seya, and M. Matsumoto. 2011. UNC93B1 physically associates with human TLR8 and regulates TLR8-mediated signaling. *PLoS ONE* 6: e28500.
11. Funami, K., M. Matsumoto, H. Oshiumi, T. Akazawa, A. Yamamoto, and T. Seya. 2004. The cytoplasmic 'linker region' in Toll-like receptor 3 controls receptor localization and signaling. *Int. Immunol.* 16: 1143–1154.
12. Nishiya, T., E. Kajita, S. Miwa, and A. L. Defranco. 2005. TLR3 and TLR7 are targeted to the same intracellular compartments by distinct regulatory elements. *J. Biol. Chem.* 280: 37107–37117.
13. Barton, G. M., J. C. Kagan, and R. Medzhitov. 2006. Intracellular localization of Toll-like receptor 9 prevents recognition of self DNA but facilitates access to viral DNA. *Nat. Immunol.* 7: 49–56.
14. Chuang, T.-H., and R. J. Ulevitch. 2000. Cloning and characterization of a sub-family of human toll-like receptors: hTLR7, hTLR8 and hTLR9. *Eur. Cytokine Netw.* 11: 372–378.
15. Du, X., A. Poltorak, Y. Wei, and B. Beutler. 2000. Three novel mammalian toll-like receptors: gene structure, expression, and evolution. *Eur. Cytokine Netw.* 11: 362–371.
16. Bell, J. K., G. E. D. Mullen, C. A. Leifer, A. Mazzoni, D. R. Davies, and D. M. Segal. 2003. Leucine-rich repeats and pathogen recognition in Toll-like receptors. *Trends Immunol.* 24: 528–533.
17. Latz, E., A. Verma, A. Visintin, M. Gong, C. M. Sirois, D. C. Klein, B. G. Monks, C. J. McKnight, M. S. Lamphier, W. P. Duprex, et al. 2007. Ligand-induced conformational changes allosterically activate Toll-like receptor 9. *Nat. Immunol.* 8: 772–779.
18. Hemmi, H., T. Kaisho, O. Takeuchi, S. Sato, H. Sanjo, K. Hoshino, T. Horiuchi, H. Tomizawa, K. Takeda, and S. Akira. 2002. Small anti-viral compounds activate immune cells via the TLR7 MyD88-dependent signaling pathway. *Nat. Immunol.* 3: 196–200.
19. Jurk, M., F. Heil, J. Vollmer, C. Schetter, A. M. Krieg, H. Wagner, G. Lipford, and S. Bauer. 2002. Human TLR7 or TLR8 independently confer responsiveness to the antiviral compound R-848. *Nat. Immunol.* 3: 499.
20. Heil, F., H. Hemmi, H. Hochrein, F. Ampenberger, C. Kirschning, S. Akira, G. Lipford, H. Wagner, and S. Bauer. 2004. Species-specific recognition of single-stranded RNA via toll-like receptor 7 and 8. *Science* 303: 1526–1529.
21. Diebold, S. S., T. Kaisho, H. Hemmi, S. Akira, and C. Reis e Sousa. 2004. Innate antiviral responses by means of TLR7-mediated recognition of single-stranded RNA. *Science* 303: 1529–1531.
22. Hemmi, H., O. Takeuchi, T. Kawai, T. Kaisho, S. Sato, H. Sanjo, M. Matsumoto, K. Hoshino, H. Wagner, K. Takeda, and S. Akira. 2000. A Toll-like receptor recognizes bacterial DNA. *Nature* 408: 740–745.
23. Krieg, A. M. 2002. CpG motifs in bacterial DNA and their immune effects. *Annu. Rev. Immunol.* 20: 709–760.
24. Matsumoto, F., S. Saitoh, R. Fukui, T. Kobayashi, N. Tanimura, K. Konno, Y. Kusumoto, S. Akashi-Takamura, and K. Miyake. 2008. Cathepsins are required for Toll-like receptor 9 responses. *Biochem. Biophys. Res. Commun.* 367: 693–699.
25. Ewald, S. E., B. L. Lee, L. Lau, K. E. Wickliffe, G. P. Shi, H. A. Chapman, and G. M. Barton. 2008. The ectodomain of Toll-like receptor 9 is cleaved to generate a functional receptor. *Nature* 456: 658–662.
26. Park, B., M. M. Brinkmann, E. Spooner, C. C. Lee, Y. M. Kim, and H. L. Ploegh. 2008. Proteolytic cleavage in an endolysosomal compartment is required for activation of Toll-like receptor 9. *Nat. Immunol.* 9: 1407–1414.
27. Sepulveda, F. E., S. Maschalidi, R. Colisson, L. Heslop, C. Ghirelli, E. Sakka, A. M. Lennon-Duménil, S. Amigorena, L. Cabanie, and B. Manoury. 2009. Critical role for asparagine endopeptidase in endocytic Toll-like receptor signaling in dendritic cells. *Immunity* 31: 737–748.
28. Ewald, S. E., A. Engel, J. Lee, M. Wang, M. Bogyo, and G. M. Barton. 2011. Nucleic acid recognition by Toll-like receptors is coupled to stepwise processing by cathepsins and asparagine endopeptidase. *J. Exp. Med.* 208: 643–651.
29. Maschalidi, S., S. Hässler, F. Blanc, F. E. Sepulveda, M. Tohme, M. Chignard, P. van Endert, M. Si-Tahar, D. Descamps, and B. Manoury. 2012. Asparagine endopeptidase controls anti-influenza virus immune responses through TLR7 activation. *PLoS Pathog.* 8: e1002841.
30. Hipp, M. M., D. Shepherd, U. Gileadi, M. C. Aichinger, B. M. Kessler, M. J. Edelmann, R. Essalmani, N. G. Seidah, C. Reis e Sousa, and V. Cerundolo. 2013. Processing of human toll-like receptor 7 by furin-like proprotein convertases is required for its accumulation and activity in endosomes. *Immunity* 39: 711–721.
31. Kanno, A., C. Yamamoto, M. Onji, R. Fukui, S. Saitoh, Y. Motoi, T. Shibata, F. Matsumoto, T. Muta, and K. Miyake. 2013. Essential role for Toll-like receptor 7 (TLR7)-unique cysteines in an intramolecular disulfide bond, proteolytic cleavage and RNA sensing. *Int. Immunol.* 25: 413–422.
32. Onji, M., A. Kanno, S. Saitoh, R. Fukui, Y. Motoi, T. Shibata, F. Matsumoto, A. Lamichhane, S. Sato, H. Kiyono, et al. 2013. An essential role for the N-terminal fragment of Toll-like receptor 9 in DNA sensing. *Nat. Commun.* 4: 1949.
33. Hornung, V., S. Rothenfusser, S. Britsch, A. Krug, B. Jahrsdörfer, T. Giese, S. Endres, and G. Hartmann. 2002. Quantitative expression of toll-like receptor 1-10 mRNA in cellular subsets of human peripheral blood mononuclear cells and sensitivity to CpG oligodeoxynucleotides. *J. Immunol.* 168: 4531–4537.
34. Peng, G., Z. Guo, Y. Kiniwa, K. S. Voo, W. Peng, T. Fu, D. Y. Wang, Y. Li, H. Y. Wang, and R. F. Wang. 2005. Toll-like receptor 8-mediated reversal of CD4+ regulatory T cell function. *Science* 309: 1380–1384.
35. Janke, M., J. Poth, V. Wimmenauer, T. Giese, C. Coch, W. Barchet, M. Schlee, and G. Hartmann. 2009. Selective and direct activation of human neutrophils but not eosinophils by Toll-like receptor 8. *J. Allergy Clin. Immunol.* 123: 1026–1033.
36. Jongbloed, S. L., A. J. Kassianos, K. J. McDonald, G. J. Clark, X. Ju, C. E. Angel, C. J. Chen, P. R. Dunbar, R. B. Wadley, V. Jeet, et al. 2010. Human CD141+ (BDCA-3)+ dendritic cells (DCs) represent a unique myeloid DC subset that cross-presents necrotic cell antigens. *J. Exp. Med.* 207: 1247–1260.
37. Sarvestani, S. T., B. R. Williams, and M. P. Gantier. 2012. Human Toll-like receptor 8 can be cool too: implications for foreign RNA sensing. *J. Interferon Cytokine Res.* 32: 350–361.
38. Fabbri, M., A. Paone, F. Calore, R. Galli, E. Gaudio, R. Santhanam, F. Lovat, P. Fadda, C. Mao, G. J. Nuovo, et al. 2012. MicroRNAs bind to Toll-like receptors to induce prometastatic inflammatory response. *Proc. Natl. Acad. Sci. USA* 109: E2110–E2116.
39. Tanji, H., U. Ohto, T. Shibata, K. Miyake, and T. Shimizu. 2013. Structural reorganization of the Toll-like receptor 8 dimer induced by agonistic ligands. *Science* 339: 1426–1429.
40. Zarember, K. A., and P. J. Godowski. 2002. Tissue expression of human Toll-like receptors and differential regulation of Toll-like receptor mRNAs in leukocytes in response to microbes, their products, and cytokines. *J. Immunol.* 168: 554–561.
41. Schmid, H., R. Sauerbrei, G. Schwarz, E. Weber, H. Kalbacher, and C. Driessen. 2002. Modulation of the endosomal and lysosomal distribution of cathepsins B, L and S in human monocytes/macrophages. *Biol. Chem.* 383: 1277–1283.
42. Matsumoto, M., and T. Seya. 2008. TLR3: interferon induction by double-stranded RNA including poly(I:C). *Adv. Drug Deliv. Rev.* 60: 805–812.
43. Garcia-Cattaneo, A., F. X. Gobert, M. Müller, F. Toscano, M. Flores, A. Lescure, E. Del Nery, and P. Benaroch. 2012. Cleavage of Toll-like receptor 3 by cathepsins B and H is essential for signaling. *Proc. Natl. Acad. Sci. USA* 109: 9053–9058.
44. Qi, R., D. Singh, and C. C. Kao. 2012. Proteolytic processing regulates Toll-like receptor 3 stability and endosomal localization. *J. Biol. Chem.* 287: 32617–32629.
45. Toscano, F., Y. Estornes, F. Virard, A. Garcia-Cattaneo, A. Pierrot, B. Vanbervliet, M. Bonnin, M. J. Ciancanelli, S. Y. Zhang, K. Funami, et al. 2013. Cleaved/associated TLR3 represents the primary form of the signaling receptor. *J. Immunol.* 190: 764–773.
46. Tatematsu, M., F. Nishikawa, T. Seya, and M. Matsumoto. 2013. Toll-like receptor 3 recognizes incomplete stem structures in single-stranded viral RNA. *Nat. Commun.* 4: 1833.
47. Li, Y., I. C. Berke, and Y. Modis. 2012. DNA binding to proteolytically activated TLR9 is sequence-independent and enhanced by DNA curvature. *EMBO J.* 31: 919–931.
48. Gringhuis, S. I., M. van der Vlist, L. M. van den Berg, J. den Dunnen, M. Litjens, and T. B. Geijtenbeek. 2010. HIV-1 exploits innate signaling by TLR8 and DC-SIGN for productive infection of dendritic cells. *Nat. Immunol.* 11: 419–426.
49. Han, X., X. Li, S. C. Yue, A. Anandaiah, F. Hashem, P. S. Reinach, H. Koziel, and S. D. Tachado. 2012. Epigenetic regulation of tumor necrosis factor α (TNFα) release in human macrophages by HIV-1 single-stranded RNA (ssRNA) is dependent on TLR8 signaling. *J. Biol. Chem.* 287: 13778–13786.
50. Saitoh, T., J. Komano, Y. Saitoh, T. Misawa, M. Takahama, T. Kozaki, T. Uehata, H. Iwasaki, H. Omori, S. Yamaoka, et al. 2012. Neutrophil extracellular traps mediate a host defense response to human immunodeficiency virus-1. *Cell Host Microbe* 12: 109–116.
51. Ablasser, A., H. Poeck, D. Anz, M. Berger, M. Schlee, S. Kim, C. Bourquin, N. Goutagny, Z. Jiang, K. A. Fitzgerald, et al. 2009. Selection of molecular structure and delivery of RNA oligonucleotides to activate TLR7 versus TLR8 and to induce high amounts of IL-12p70 in primary human monocytes. *J. Immunol.* 182: 6824–6833.

52. Marshak-Rothstein, A. 2006. Toll-like receptors in systemic autoimmune disease. *Nat. Rev. Immunol.* 6: 823–835.
53. Krieg, A. M., and J. Vollmer. 2007. Toll-like receptors 7, 8, and 9: linking innate immunity to autoimmunity. *Immunol. Rev.* 220: 251–269.
54. Demaria, O., P. P. Pagni, S. Traub, A. de Gassart, N. Branzk, A. J. Murphy, D. M. Valenzuela, G. D. Yancopoulos, R. A. Flavell, and L. Alexopoulou. 2010. TLR8 deficiency leads to autoimmunity in mice. *J. Clin. Invest.* 120: 3651–3662.
55. Guiducci, C., M. Gong, A.-M. Cepika, Z. Xu, C. Tripodo, L. Bennett, C. Crain, P. Quartier, J. J. Cush, V. Pascual, et al. 2013. RNA recognition by human TLR8 can lead to autoimmune inflammation. *J. Exp. Med.* 210: 2903–2919.
56. Kokkinopoulos, I., W. J. Jordan, and M. A. Ritter. 2005. Toll-like receptor mRNA expression patterns in human dendritic cells and monocytes. *Molec. Immunol.* 42: 957–968.

INAM Plays a Critical Role in IFN-γ Production by NK Cells Interacting with Polyinosinic-Polycytidylic Acid–Stimulated Accessory Cells

Jun Kasamatsu,* Masahiro Azuma,*,[1] Hiroyuki Oshiumi,* Yuka Morioka,[†] Masaru Okabe,[‡] Takashi Ebihara,*,[2] Misako Matsumoto,* and Tsukasa Seya*

Polyinosinic-polycytidylic acid strongly promotes the antitumor activity of NK cells via TLR3/Toll/IL-1R domain–containing adaptor molecule 1 and melanoma differentiation-associated protein-5/mitochondrial antiviral signaling protein pathways. Polyinosinic-polycytidylic acid acts on accessory cells such as dendritic cells (DCs) and macrophages (Mφs) to secondarily activate NK cells. In a previous study in this context, we identified a novel NK-activating molecule, named IFN regulatory factor 3–dependent NK-activating molecule (INAM), a tetraspanin-like membrane glycoprotein (also called Fam26F). In the current study, we generated INAM-deficient mice and investigated the in vivo function of INAM. We found that cytotoxicity against NK cell–sensitive tumor cell lines was barely decreased in *Inam*$^{-/-}$ mice, whereas the number of IFN-γ–producing cells was markedly decreased in the early phase. Notably, deficiency of INAM in NK and accessory cells, such as CD8α$^+$ conventional DCs and Mφs, led to a robust decrease in IFN-γ production. In conformity with this phenotype, INAM effectively suppressed lung metastasis of B16F10 melanoma cells, which is controlled by NK1.1$^+$ cells and IFN-γ. These results suggest that INAM plays a critical role in NK-CD8α$^+$ conventional DC (and Mφ) interaction leading to IFN-γ production from NK cells in vivo. INAM could therefore be a novel target molecule for cancer immunotherapy against IFN-γ–suppressible metastasis. *The Journal of Immunology*, **2014, 193: 5199–5207.**

Microbial components play a major role in activating innate and adaptive immune responses by triggering pattern recognition receptors. Nucleic acid adjuvants, including polyinosinic-polycytidylic acid (polyI:C) and unmethylated CpG dinucleotides, strongly promote Th1 immune responses against cancer and infected cells and induce type I IFN and other inflammatory cytokines (1, 2). PolyI:C strongly enhances priming and expansion of Ag-specific T cells and NK cells with dramatic regression of syngeneic implant tumors in mice (3–6). NK cells belong to group 1 innate lymphocytes (ILC1s) and control progression of several types of tumors and microbial infections (7). Although polyI:C (an analog of viral dsRNA) is a ligand for multiple receptors, including dsRNA-dependent protein kinase, retinoic acid–inducible gene-I, melanoma differentiation–associated protein-5 (MDA5), and TLR3, both of the pathways initiated by TLR3/Toll/IL-1R domain–containing adaptor molecule 1 (TICAM-1) and MDA5/mitochondrial antiviral signaling protein confer antitumor activity on NK cells in vivo (8, 9).

PolyI:C also directly and indirectly activates human NK cells and other ILC1s (10, 11). PolyI:C participates in secondary activation of murine NK cells through stimulation of accessory cells such as dendritic cells (DCs) and other myeloid cells (12–14). In these interactions, previous studies have shown that type I IFN and cell contact via IL-15 receptors play a critical role in accessory cell activation followed by NK activation (15). In contrast, our previous studies showed that polyI:C induced bone marrow–derived DC (BMDC)–mediated NK cell activation through the TLR3/TICAM-1/IFN regulatory factor 3 (IRF3) pathway, which promoted antitumor immunity by adoptive transfer in a type I IFN- and IL-15–independent manner (8, 16). As the key molecule for this NK–DC interaction, we identified a novel IRF3-inducible tetraspanin-like membrane glycoprotein, named IRF3-dependent NK-activating molecule (INAM). INAM expression was induced not only in myeloid DCs but also in NK cells by polyI:C stimulation in vivo. Transfection of INAM in both BMDC and NK cells cooperated in inducing IFN-γ production and cytotoxicity against the NK-sensitive B16D8 cell line.

To investigate the role of INAM in vivo, we generated INAM-deficient mice by the standard gene-targeting method. INAM expression was induced not only in NK cells and conventional DC

*Department of Microbiology and Immunology, Graduate School of Medicine, Hokkaido University, Sapporo 060-8638, Japan; [†]Division of Disease Model Innovation, Institute for Genetic Medicine, Hokkaido University, Sapporo 060-8638, Japan; [‡]Research Institute for Microbial Disease, Osaka University, Osaka 565-0871, Japan

[1]Current address: Department of Pathology and Cellular Biology, Faculty of Medicine, University of Montreal, Montreal, QC, Canada.

[2]Current address: Department of Medicine, Howard Hughes Medical Institute, Washington University School of Medicine, St. Louis, MO.

Received for publication April 11, 2014. Accepted for publication September 9, 2014.

This work was supported in part by grants-in-aid from the Ministry of Education, Culture, Sports, Science and Technology and the Ministry of Health, Labor and Welfare of Japan, a Ministry of Education, Culture, Sports, Science and Technology of Japan Grant-in-Aid Project for Basic Research, "Carcinogenic Spiral," and the National Cancer Center Research and Development Fund (23-A-44). This work was also supported by the Takeda Science Foundation, the Yasuda Cancer Research Foundation, and the Iskra Foundation. J.K. is a Research Fellow of the Japan Society for the Promotion of Science.

Address correspondence and reprint requests to Prof. Tsukasa Seya, Department of Microbiology and Immunology, Graduate School of Medicine, Hokkaido University, Kita 15, Nishi 7, Kita-ku, Sapporo 060-8638, Japan. E-mail address: seya-tu@pop.med.hokudai.ac.jp

The online version of this article contains supplemental material.

Abbreviations used in this article: BMDC, bone marrow–derived DC; BST2, bone marrow stromal cell Ag 2; cDC, conventional DC; DC, dendritic cell; IFNAR1, IFN (α and β) receptor 1; ILC1, group 1 innate lymphocyte; INAM, IFN regulatory factor 3–dependent NK-activating molecule; IRF, IFN regulatory factor; Mφ, macrophage; MDA5, melanoma differentiation–associated protein-5; pDC, plasmacytoid DC; polyI:C, polyinosinic-polycytidylic acid; qPCR, quantitative real-time PCR; TICAM-1, Toll/IL-1R domain–containing adaptor molecule 1; WT, wild-type.

www.jimmunol.org/cgi/doi/10.4049/jimmunol.1400924

(cDC) subsets but also in other immune cells including macrophages (Mφs) and plasmacytoid DCs (pDCs) by polyI:C stimulation. Cytotoxicity against NK cell–sensitive tumor cell lines was barely decreased in *Inam*$^{-/-}$ mice, whereas the number of IFN-γ–producing cells markedly decreased in the early phase. We also showed that CD8α$^+$ cDCs and Mφs facilitate secretion of IFN-γ from NK cells in response to polyI:C stimulation in vitro and in vivo. Notably, deficiency of INAM on NK and their accessory cells led to a robust decrease in IFN-γ production. Therefore, these results infer that INAM plays a critical role in the interaction of NK-CD8α$^+$ cDCs (and Mφs) leading to IFN-γ production from NK cells. In agreement with this suggested phenotype, INAM effectively suppressed lung metastasis of B16F10 melanoma cells by controlling activation of NK1.1$^+$ cells and IFN-γ. Taken together, these results provide the first demonstration, to our knowledge, that INAM plays a critical role in the interaction of NK–CD8α$^+$ cDCs, which allows NK cells to produce IFN-γ. We propose in this study that INAM is a novel target molecule for immunotherapy against IFN-γ–suppressible tumors.

Materials and Methods

Mice

All mice were backcrossed with C57BL/6 mice more than seven times before use. A C57BL/6 background *Inam* (*Fam26f*)–targeted embryonic stem cell line, JM8A3.N1 of FAM26F tm2a (European Conditional Mouse Mutagenesis Program) Wtsi, was purchased from the European Conditional Mouse Mutagenesis Program. Chimeric mice were generated by aggregation of the mutated embryonic stem cells at the 8 cell stage. To remove exon 2 of *Inam*, the *Inam* heterozygous mutants were crossed with Cre-transgenic mice. The *Inam* heterozygous mutants obtained were intercrossed to obtain *Inam* homozygous mutants. *Ticam-1*$^{-/-}$ and *Mavs*$^{-/-}$ mice were generated in our laboratory (8, 16). *Irf-3*$^{-/-}$ and *Ifnar1*$^{-/-}$ mice were provided by Dr. T. Taniguchi (17). *Batf3*$^{-/-}$ C57BL/6 mice were purchased from The Jackson Laboratory (Bar Harbor, ME) (18). The *Batf3*$^{-/-}$ mice of C57BL/6 background [unlike 129 and BALB/c background (19)] lacked splenic CD8a$^+$ DCs as described previously (18) and evoked insufficient T cell functional response against extrinsic Ag and adjuvant (Azuma et al., submitted for publication). C57BL/6 background were purchased from CLEA Japan (Shizuoka, Japan). Experiments were performed with sex-matched mice at 8–14 wk of age. All mice were bred and maintained under specific pathogen-free conditions in the animal facility of the Hokkaido University Graduate School of Medicine. Animal experimental protocols and guidelines were approved by the Animal Safety Center, Hokkaido University.

Semiquantitative RT-PCR and quantitative real-time PCR

Total RNA was extracted using TRIzol according to the manufacturer's instructions (Invitrogen). cDNA was generated by using the High Capacity cDNA Transcription Kit (ABI) with random primers according to the manufacturer's instructions. Quantitative real-time PCR (qPCR) was performed using the Step One Real-Time PCR system (ABI). The primer sequences for qPCR analysis were 5′-CAACTGCAATGCCACGCTA-3′ and 5′-TCCAACCGAACACCTGAGACT-3′ for *Inam*; 5′-TTAACTGAGGCTGGCATTCATG-3′ and 5′-ACCTACACTGACACAGCCCAAA-3′ for *Il15*; 5′-GACAAAGAAAGCCGCCTCAA-3′ and 5′-ATGGCAGCCATTGTTCCTG-3′ for *Il18*; 5′-ACCGTGTTTACGAGGAACCCTA-3′ and 5′-GGTGAGAGCTGGCTGTTGAG-3′ for *Irf7*; 5′-GCCGAGACACAGGCAAAC-3′ and 5′-CCAGGGCTTGAGACACCTTC-3′ for bone marrow stromal cell Ag 2 (*Bst2*); and 5′-GCCTGGAGAAACCTGCCA-3′ and 5′-CCCTCAGATGCCTGCTTCA-3′ for *Gapdh*. The primer sequences for semi-qPCR analysis were 5′-CAACTGCAATGCCACGCTA-3′ and 5′-TCCAACCGAACACCTGAGACT-3′ for *Gapdh*.

Mφ depletion and stimulation using TLR agonists in vivo

To generate Mφ-depleted mice, mice were injected i.p. with 150 μl Clophosome-Clodronate Liposomes (FormuMax). For qPCR analysis of *Inam* induction using some TLR antagonists in Fig. 1E, mice were injected i.p. with 50 μg polyI:C (GE Bioscience), 50 μg Pam3CSK4 (Boehringer Ingelheim), 10 μg LPS (Sigma-Aldrich), 50 μg R837 (InvivoGen), and 50 μg CpG ODN1826 (InvivoGen). In other experiments, polyI:C was injected i.p. at a dose of 200 μg/mouse.

Cells

For isolation of DC subsets, Mφs and NK cells, spleens were treated with 400 Mandle U/ml collagenase D (Roche) at 37°C for 25 min in HBSS (Sigma-Aldrich). EDTA was added, and the cell suspension was incubated for an additional 5 min at 37°C. NK cells were purified from spleens by positive selection of DX5-positive cells with DX5 MACS beads (Miltenyi Biotec). CD8α$^+$ cDCs were purified using a CD8α$^+$ DC isolation kit and CD11c MACS beads (Miltenyi Biotec). CD8α$^-$ cDCs were purified with CD11c MACS beads (Miltenyi Biotec) from the negative fraction after CD8α$^+$ cDC separation. F4/80$^+$ Mφs were isolated using MACS-positive selection beads (Miltenyi Biotec) as described previously (13). pDC Ag-1$^+$ pDCs were isolated with pDC Ag-1 MACS beads (Miltenyi Biotec). All immune cells were purified from spleens by repeated positive selection to achieve high purity (90%). Leukocytes from the lung were prepared as previously reported (18). Mouse immune cells were cultured in RPMI 1640/10% FCS/55 μM 2-ME/10 mM HEPES. B16D8, B16F10, YAC-1, and RMA-S were cultured in RPMI 1640/10% FCS.

Cell culture

To investigate potential interactions with NK–accessory cells, MACS-sorted accessory cells were cocultured with freshly isolated NK cells (accessory cells /NK = 1:2) with or without 20 μg/ml polyI:C for 24 h. In some coculture experiments using the transwell system, NK cells were added to 0.4-μm pore transwells (Corning) in the presence of polyI:C. Activation of NK cells was assessed by measuring the concentration of IFN-γ (ELISA; GE Healthcare) in the medium. For the IFN (α and β) receptor 1 (IFNAR1) blocking experiment, anti-IFNAR Ab at a final concentration of 10 μg/ml was added to the cultures before addition of polyI:C. For measurement of IL-12p40 and type I IFNs, we used ELISA kits purchased from BioLegend and PBL Biomedical Laboratories, respectively.

FACS analysis

For intracellular cytokine staining of NK cells, we isolated spleen or lung from polyI:C- or PBS-injected mice at each time point and harvested their leukocytes as described previously (18, 19). The leukocytes were incubated in medium with 10 μg/ml brefeldin A for 4 h. Cells were fixed and stained with a combination of anti-NK1.1 (PK136) and anti-CD3ε (145-2C11) Abs (BioLegend), followed by permeabilization and staining with anti-IFN-γ (XMG1.2) Ab (BioLegend), anti–granzyme B (NGZB) Ab (eBioscience), anti–TNF-α (MP6-XT22) Ab (BioLegend), anti–GM-CSF (MP1-22E9) Ab (BioLegend), or anti–IL-2 (JES6-5H4) Ab (BioLegend) using a BD Cytofix/Cytoperm Kit (BD Biosciences). For staining of the C terminus of INAM of each immune cell type, after treatment of anti-CD16/32 (no. 93), cell-surface molecules of splenocytes were stained with anti-CD3ε (145-2C11), anti-CD8α (53-6.7), anti-CD11c (N418), anti-NK1.1, anti-F4/80 (BM8), anti-Gr1 (RB6-8C5), anti-CD11b (M1/70), or anti-CD19 (MB19-1) Abs (BioLegend) or with anti-B220 (RA3-6B2) or anti-CD4 (L3T4) Abs (eBioscience). After staining of the cell surface, cells were fixed and permeabilized using a BD Cytofix/Cytoperm Kit (BD Biosciences) and then stained with an anti-INAM polyclonal Ab as described previously (16). To detect activating markers, NK receptors, and developmental markers, splenocytes were stained with anti-CD27 (LG.3A10), anti-CD25 (PC61), anti-NKp46 (29A1.4), anti-NKG2D (C7), anti-DNAM-1 (10E5), and anti-TRAIL (N2B2) Abs from BioLegend or anti-Fas (Jo2) from BD Biosciences. For detection of dead cells, samples were stained with ViaProbe from BD Biosciences. Samples were processed on an FACSCalibur flow cytometer and analyzed with FlowJo software (Tree Star).

Tumor inoculation and polyI:C treatment

PolyI:C therapy against mice with B16D8 tumor burden was described previously (8). B16F10 melanoma cells (2×10^5) were injected into wild-type (WT) or *Inam*$^{-/-}$ mice via the tail vein on day 0. PolyI:C was injected i.p. on days 1, 4, 7, and 10 at a dose of 200 μg/mouse. The control group was treated with PBS. All mice were killed 12 d after tumor inoculation. The lungs were excised and fixed in Mildform (Wako) for counting of surface colonies under a dissection microscope.

Statistical analysis

Statistical analyses were made with the Student *t* test for paired data. Statistical analyses were made with ANOVA in multiple comparisons. The *p* value of significant differences is reported.

Results

Generation of INAM-deficient mice

We designed a targeting vector to disrupt exon 2, which encodes the C-terminal transmembrane and cytoplasmic regions of INAM

(Fig. 1A). The heterozygosity and homozygosity of siblings were verified by Southern blot analysis (Fig. 1B). Mutant mice were born at the expected Mendelian ratio from *Inam*$^{-/-}$ and *Inam*$^{+/-}$ parents and showed normal healthy development under specific pathogen-free conditions (Fig. 1C). We also examined the composition of immune cells in the spleen and found no clear difference between WT and *Inam*$^{-/-}$ mice (Table I). Murine NK cells are divided into four subsets in their maturation stage based on the surface density of CD27 and CD11b: CD11b^{low}/CD27^{low}, CD11b^{low}/CD27^{high}, CD11b^{high}/CD27^{high}, and CD11b^{high} /CD27^{low} (20). We examined the composition of splenic NK cells in each maturation stage and found no clear difference between WT and *Inam*$^{-/-}$ mice (Supplemental Fig. 1A). A previous study showed that *Inam* mRNA is highly expressed in spleen and thymus under steady-state conditions

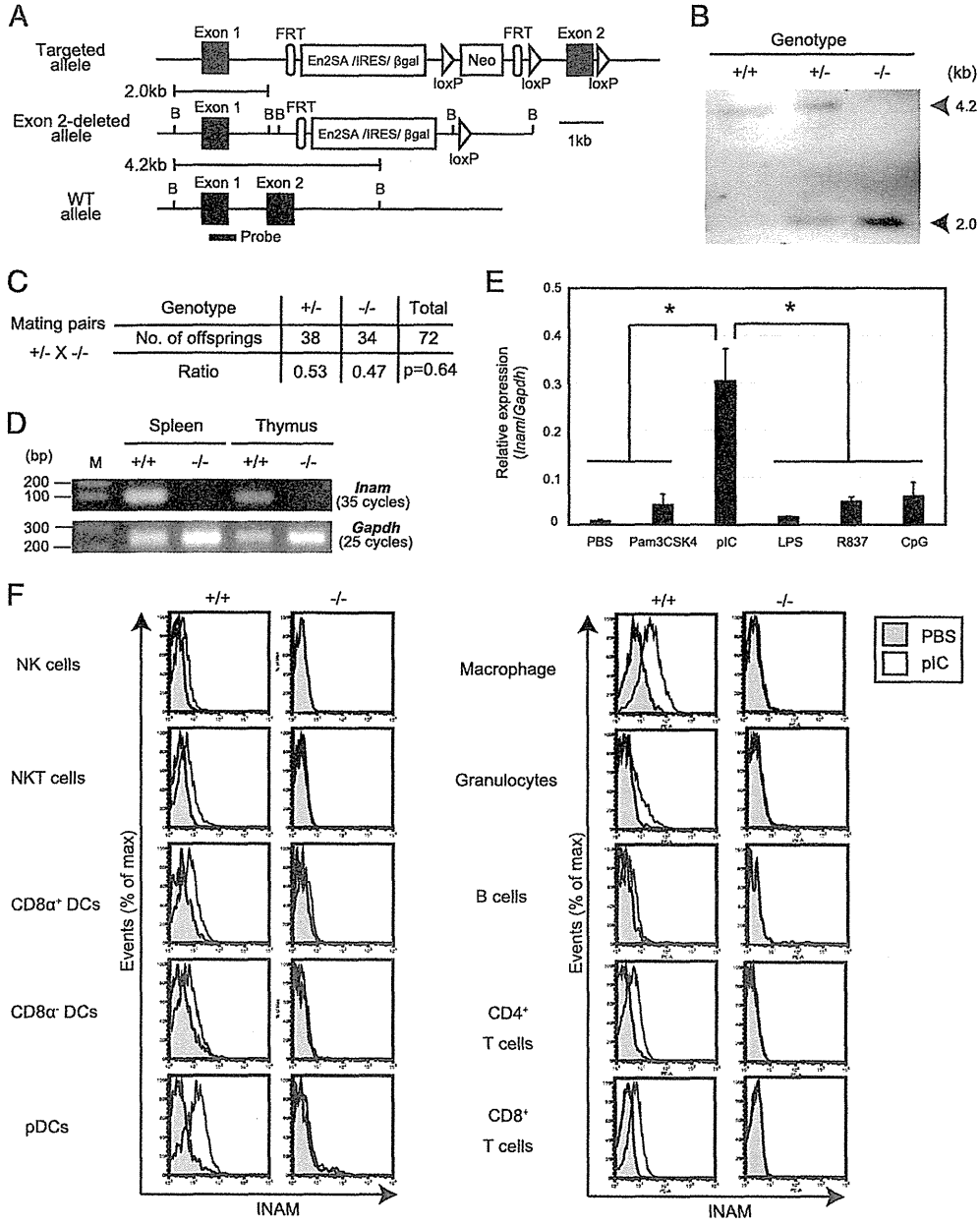

FIGURE 1. Generation of INAM-deficient mice. (**A**) Structure of the mouse *Inam*-targeted, *Inam*-disrupted, and WT allele. Closed boxes indicate the coding exon of Inam. A probe (602 bp) for Southern blot analysis was designed in exon 1. (**B**) Southern blot analysis of BamHI-digested genomic DNA isolated from WT (+/+), heterozygous mutant (+/−), and homozygous mutant (−/−) mice. (**C**) Genotype analyses of offspring from heterozygote intercrosses. The χ^2 goodness-of-fit test indicated that deviation from the Mendelian ratio was not statistically significant ($p > 0.1$). (**D**) RT-PCR analysis of spleen and thymus. Total RNA sets from spleen and thymus in WT (+/+) and *Inam*$^{-/-}$ (−/−) mice were extracted and subjected to RT-PCR to determine *Inam* expression. (**E**) *Inam* mRNA expression in response to TLR agonists. Total RNA were isolated from the spleens of mice in each group ($n = 3$) at 3 h after TLR agonist stimulation and subjected to quantitative PCR to determine to determine *Inam* expression. *$p < 0.05$ (**F**) INAM expression of immune cells. WT (+/+) and *Inam*$^{-/-}$ (−/−) mice were i.p. injected with 200 μg polyI:C (pIC) or PBS ($n = 2$). After 12 h, INAM expression of each immune cell type was analyzed by flow cytometry. Open histograms and shaded histograms indicate immune cells derived from the mice. Immune cells were classified as NK cells (CD3ε$^-$/NK1.1$^+$), NKT cells (CD3ε$^-$/NK1.1^{int}), B cells (CD19c$^+$/B220$^+$), CD8$^+$ T cells (CD3ε$^+$/CD8α$^+$), CD4$^+$ T cells (CD3ε$^+$/CD4α$^+$), classic CD8α$^-$ cDCs (CD11c^{high}/CD8α$^-$), classic CD8α$^+$ cDCs (CD11c^{high}/CD8α$^+$), pDCs (CD11c^{int}/B220$^+$), Mφs (CD11c$^{low\text{-}dim}$/CD11b$^{low\text{-}dim}$/F4/80$^+$), and granulocytes (CD11b^{high}/Gr-1$^+$). The data shown are representative of at least two independent experiments.

Table I. Development of hematopoietic cells in INAM-deficient mice

Cells	WT	*Inam*$^{-/-}$	Student *t* Test
CD4$^+$ T cells	16.9 ± 0.3	16.2 ± 2.2	$p = 0.69$
CD8$^+$ T cells	8.6 ± 0.5	8.0 ± 1.0	$p = 0.27$
B cells	55.6 ± 1.9	56.4 ± 3.5	$p = 0.65$
NK cells	1.2 ± 0.4	2.3 ± 0.7	$p = 0.22$
NKT cells	0.9 ± 0.1	0.76 ± 0.2	$p = 0.27$
pDCs	1.0 ± 0.1	1.0 ± 0.1	$p = 0.91$
CD8α$^+$ DCs	0.2 ± 0.01	0.3 ± 0.02	$p = 0.03$
CD8α$^-$ DCs	0.49 ± 0.03	0.8 ± 0.2	$p = 0.09$
Granulocytes	0.3 ± 0.04	1.0 ± 1.2	$p = 0.43$
Mφ	1.8 ± 0.6	2.2 ± 0.8	$p = 0.45$
Resident monocytes	0.4 ± 0.1	0.4 ± 0.1	$p = 0.96$
Inflammatory monocytes	0.2 ± 0.03	0.2 ± 0.2	$p = 0.82$

Data are percentages unless otherwise indicated.

(16). In our study, mRNA expression of *Inam* in these tissues was clearly absent in the *Inam*-null mouse (Fig. 1D). To assess the induction of *Inam* mRNA expression in response to TLR agonists in vivo, we performed qPCR analysis using spleens at 3 h after i.p. administration of those agonists or PBS. The levels of *Inam* mRNA expression was strongly induced by polyI:C, but not other TLR agonists (Fig. 1E). Hence, these data indicate that polyI:C is the strongest TLR agonist to induce *Inam* expression of the TLR agonists tested in vivo. To investigate the cellular distribution of INAM protein expression, we performed flow cytometric analysis using polyclonal Abs to mouse INAM after i.p. administration of polyI:C. The levels of INAM protein expression in these cells clearly reflected the absence of the mRNA (Fig. 1F). Flow cytometric analysis of spleen cells demonstrated that INAM expression was induced in all myeloid lineage cells, including DC subsets and NK cells. In particular, INAM expression was highly induced in pDCs and F4/80$^+$ Mφs.

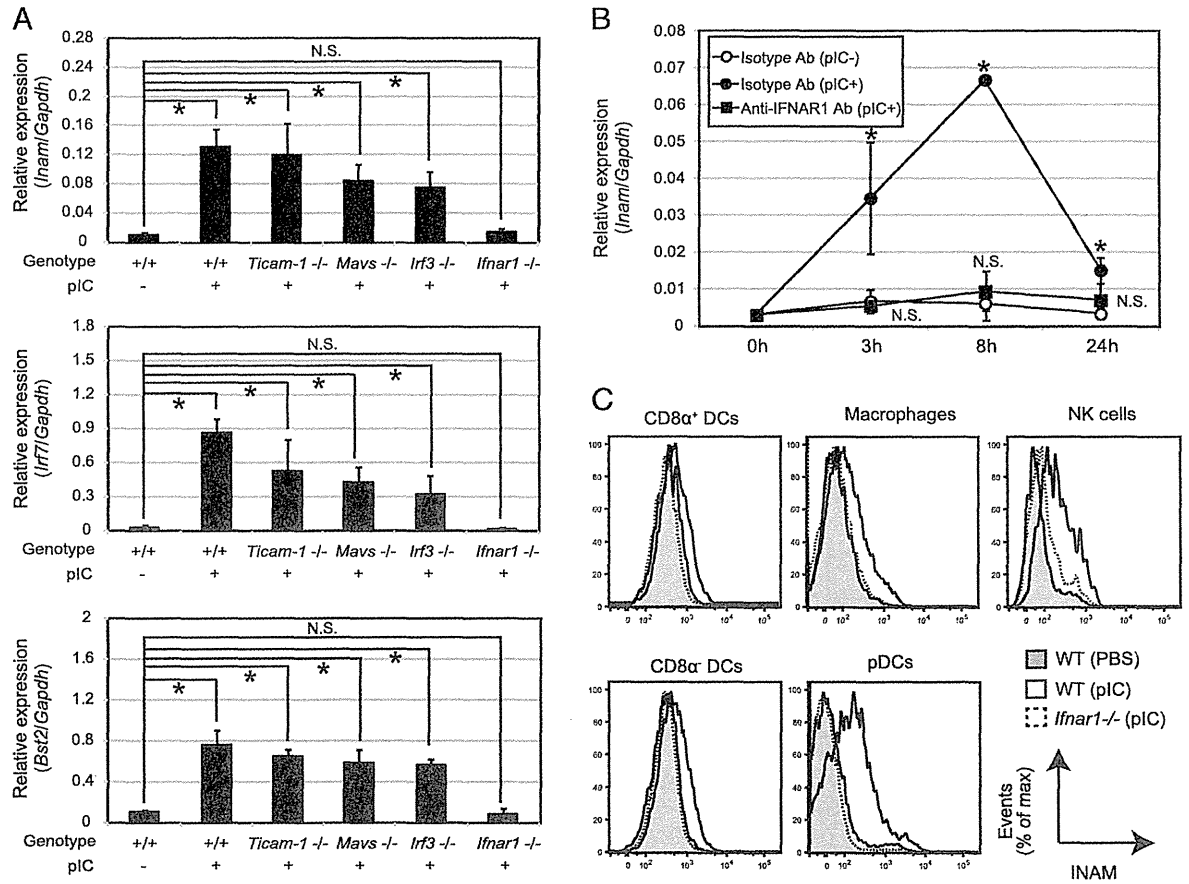

FIGURE 2. Signaling pathway of INAM induction in vivo. **(A)** *Inam* expression in splenocytes derived from various gene-manipulated mice. After 3 h, total RNA were isolated from the spleens of mice in each group ($n = 3$) and subjected to quantitative PCR to determine *Inam*, *Irf7*, and *Bst2* expression. **(B)** Type I IFN signaling is required for *Inam* expression of splenocytes derived from WT mice. Splenocytes ($n = 3$) were treated with polyI:C (pIC), IFNAR1-blocking Ab, or isotype control Ab for 0, 3, 8, and 24 h. **(C)** Type I IFN signaling is required for INAM expression of DC subsets, NK cells, and Mφs. WT and *Ifnar1*$^{-/-}$ mice were i.p. injected with 200 μg polyI:C or PBS ($n = 2$). After 12 h, INAM expression of each immune cell type was analyzed by flow cytometry. The data shown are representative of at least two independent experiments. Data are means ± SD of three independent samples. *$p < 0.05$.

Type I IFN signaling is required for INAM induction in vivo

The TLR3/TICAM-1 and MDA5/mitochondrial antiviral signaling protein pathways activate the transcription factor IRF3 in response to viral RNA. In BMDC, polyI:C (an analog of virus dsRNA) directly induces INAM expression via the TICAM-1/IRF3 pathway (16). Moreover, in the absence of pattern recognition receptor signals, IFN-α stimulation triggers INAM expression in BMDC. However, it is unclear which innate signal is required for its up-regulation in vivo. To understand the inducible pathway of *Inam* expression, we investigated its expression in spleen cells derived from various genetically manipulated mice. After polyI:C stimulation, *Inam* expression was completely undetectable in IFN (α and β) receptor 1 $(Ifnar1)^{-/-}$ mice, but not in $Ticam\text{-}1^{-/-}$ mice, a similar pattern of expression to that seen in type I IFN–inducible genes including *Irf7* and *Bst2* (Fig. 2A). Additionally, *Inam* expression was partially reduced in mice deficient in *Mavs* or *Irf3*, factors that are critical for producing type I IFN in response to polyI:C (3, 16). To assess the effect of type I IFN in WT mice, splenocytes were stimulated with polyI:C in the presence of anti-IFNAR1 Ab or isotype control Ab. Expression of *Inam* was transient, peaking at 8 h in the stimulated group in the presence of isotype control Ab (Fig. 2B). In contrast, blocking of the type I IFN receptor led to abrogation of *Inam* induction. In agreement with these results, INAM protein expression was completely undetectable in DC subsets, NK cells, and Mφs derived from IFNAR1-deficient mice (Fig. 2C). Hence, these data indicate that INAM expression depends on the IFNAR1 signaling pathway in vivo.

INAM is required for IFN-γ production through NK–accessory interaction

To identify the accessory cells directly responding to polyI:C and leading to IFN-γ production from NK cells, we performed an experiment on a coculture consisting of MACS-sorted splenic NK cells and myeloid immune cells including DC subsets and Mφs. Purified NK cells cultured in medium with or without polyI:C did not produce IFN-γ (Fig. 3A). In contrast, a high level of IFN-γ production was observed in the supernatant of NK cells cocultured with $CD8\alpha^+$ cDCs and Mφs in the presence of polyI:C, but not in pDCs and $CD8\alpha^-$ cDCs. In our reports, cell-to-cell contact is required for the interaction between NK cells and BMDC (8, 16). To confirm that the cell-to-cell contact is a prerequisite for the interaction between NK cells and splenic accessory cells, we performed coculture experiments using transwell system. As

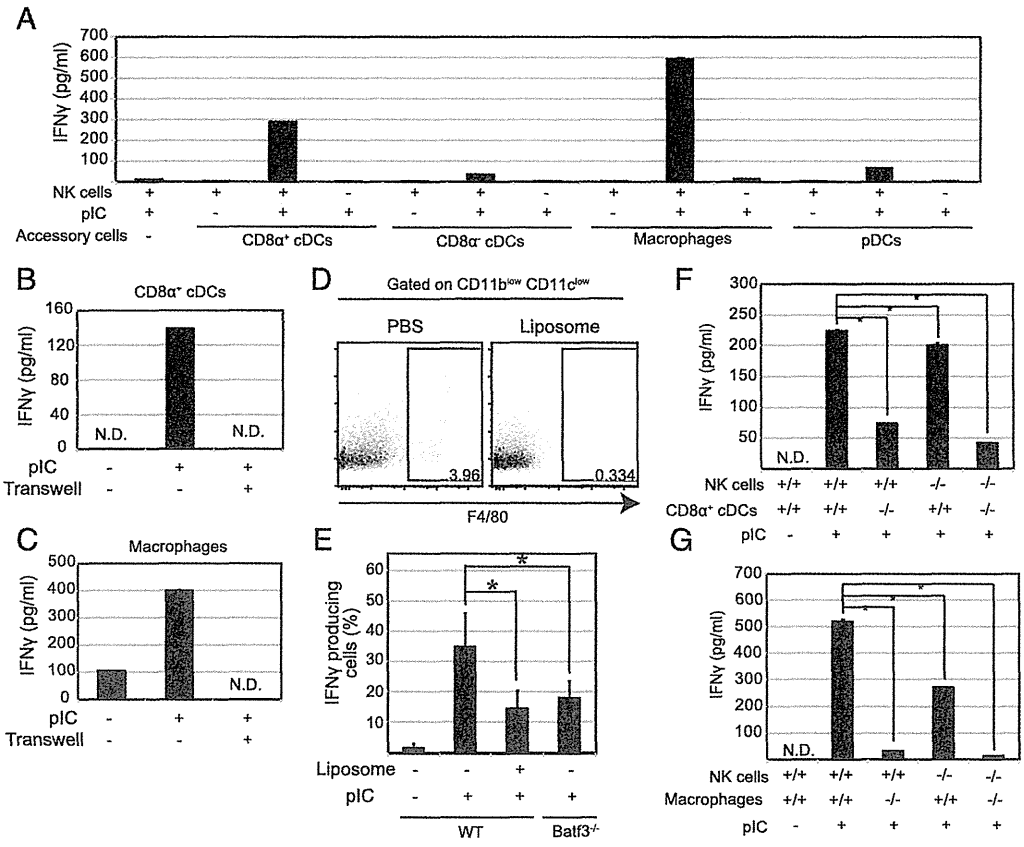

FIGURE 3. INAM-dependent NK cell activation in vitro. (**A**) IFN-γ production of NK cells via polyI:C (pIC)-stimulated DC subsets and Mφs. NK cells, DC subsets, and Mφs were enriched by MACS separation from WT and $Inam^{-/-}$ mice. (**B**) Cell-to-cell contact-dependent NK cell activation via $CD8\alpha^+$ cDCs. (**C**) Cell-to-cell contact-dependent NK cell activation via Mφs. NK cells were cocultured with DC subsets and Mφs in the presence of polyI:C (20 μg/ml) for 24 h. The concentrations of IFN-γ in the culture supernatants were measured by ELISA. (**D**) Mφ depletion with clodronate liposomes. WT mice were i.p. injected with clodronate liposomes (150 μl/mouse) to remove Mφs. After 24 h, the efficiency of Mφ depletion was measured by FACS analysis. (**E**) Production of IFN-γ by NK cells in WT, Mφ-depleted WT, and $Batf3^{-/-}$ mice. WT, Mφ-depleted WT, and $Batf3^{-/-}$ mice were i.p. injected with 200 μg polyI:C ($n = 3$). After 3 h, splenocytes were isolated, cultured with brefeldin A for an additional 4 h, and analyzed for intracellular content of IFN-γ by FACS, gating on $CD3\varepsilon^-$/$NK1.1^+$ cells. (**F**) INAM-dependent NK cell activation via $CD8\alpha^+$ cDCs. (**G**) INAM-dependent NK cell activation via Mφs. NK cells, $CD8\alpha^+$ cDCs, and Mφs were enriched via MACS separation from WT and $Inam^{-/-}$ mice. NK cells were cocultured with $CD8\alpha^+$ cDCs or Mφs in the presence of polyI:C (20 μg/ml) for 24 h. The concentrations of IFN-γ in the culture supernatants were measured by ELISA. The data shown are representative of at least two independent experiments. Data are means ± SD of three independent samples. $^*p < 0.05$.

a result, IFN-γ production was completely blocked under transwell conditions (Fig. 3B, 3C). Therefore, NK cells are primed through contact with CD8α$^+$ cDCs and Mφs independent of soluble mediators. To directly test the contribution of CD8α$^+$ cDCs and Mφs to polyI:C-mediated NK cell activation in vivo, we analyzed *Batf3*$^{-/-}$ mice, which largely lack the CD8α$^+$ cDC population in the spleen of C57BL/6 mice (21), and Mφ-depleted mice generated by clodronate liposome injection (22, 23). Approximately 85% of Mφs were depleted at 24 h after clodronate liposome injection (Fig. 3D). Three hours after polyI:C stimulation, NK cell secretion of IFN-γ was partially decreased in *Batf3*$^{-/-}$ and Mφ-depleted mice (Fig. 3E). These results indicate that CD8α$^+$ cDCs and Mφs are responsible for secretion of IFN-γ from NK cells in response to polyI:C stimulation.

INAM acts on NK cells and BMDC to orchestrate NK–DC interaction triggered by polyI:C stimulation (16). To investigate the role of INAM in the interaction of NK-CD8α$^+$ cDC and NK-Mφ, we performed an experiment on a coculture of MACS-sorted splenic NK cells with their accessory cells isolated from WT and *Inam*$^{-/-}$ mice. Cocultures of NK cells and accessory cells lacking INAM showed that IFN-γ production from NK cells required INAM expression in either NK cells or accessory cells (Fig. 3F, 3G). Notably, deficiency of INAM in both NK and accessory cells led to a marked decrease in IFN-γ production. Taken together, these results suggest that INAM is required for cell–cell contact in both NK cells and accessory cells and early IFN-γ production by NK cells.

INAM plays a critical role in rapid IFN-γ production by NK cells in response to polyI:C in vivo

To investigate the role of INAM in polyI:C-mediated cytotoxicity of NK cells, we injected WT and *Inam*$^{-/-}$ mice with polyI:C. After 0, 3, and 24 h, we isolated splenic NK cells and measured cytotoxicity ex vivo. In the four NK-sensitive cell lines B16D8, RMA-S, B16F10, and YAC-1, we found no difference between WT and *Inam*$^{-/-}$ mice in the cytotoxic effect of NK cells against these cell lines (data not shown). Consistent with these results, cell numbers expressing granzyme B, known as a cytotoxic lymphocyte protease, barely differed between splenocytes of WT and *Inam*$^{-/-}$ mice (Fig. 4A). To determine the role of INAM in NK cell production of IFN-γ in response to polyI:C, we isolated splenocytes 0, 1, and 3 h after injecting WT and *Inam*$^{-/-}$ mice with polyI:C and determined the intracellular content of IFN-γ in NK cells. After 3 h, NK cells isolated from *Inam*$^{-/-}$ mice produced less IFN-γ than WT NK cells (Fig. 4B). Additionally, we also measured the numbers of other cytokine-producing cells, including GM-CSF, IL-2, and TNF-α, from NK cells at 3 h after polyI:C stimulation in WT and *Inam*$^{-/-}$ mice and confirmed no INAM dependence of the production of these cytokines (Supplemental Fig. 2A). Therefore, INAM specifically regulates IFN-γ through CD8α DC at least within this time frame. We also measured CD69 expression, known as an NK-activating marker at 0, 3, and 24 h after polyI:C stimulation. CD69 upregulation in response to polyI:C was partially impaired in NK cells from *Inam*$^{-/-}$ mice in comparison with those from WT mice 24 h after polyI:C stimulation (Fig. 4C). We found no clear difference between WT and *Inam*$^{-/-}$ mice in expression of CD27 or NK1.1, both of which evoke IFN-γ production through their interaction with the ligands, or in any other NK receptors at 0, 3, and 24 h after polyI:C injection (24) (Supplemental Fig. 1B). These results indicate that INAM-mediated NK activation is independent of incremental expression of these receptors. Previous reports suggested that proinflammatory cytokines including IL-12, IL-15, IL-18, and type I IFN play critical roles in the cytotoxicity and IFN-γ production of NK cells (15, 25, 26). To determine their expression at 0, 3, and 24 h

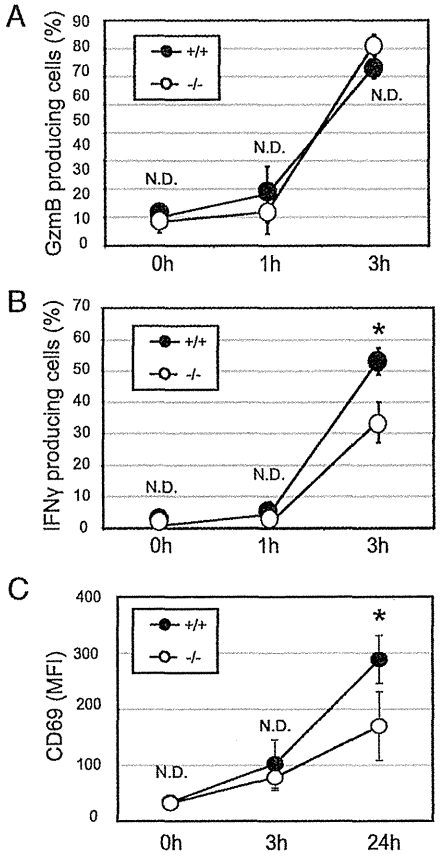

FIGURE 4. INAM-dependent NK cell activation in vivo. (**A**) Production of granzyme B (GzmB) by NK cells. (**B**) Production of IFN-γ by NK cells. WT (+/+) and *Inam*$^{-/-}$ (−/−) mice were i.p. injected with 200 μg polyI:C. After 0, 1, and 3 h, splenocytes were isolated, cultured with brefeldin A for an additional 4 h, and analyzed for intracellular content of IFN-γ and granzyme B by FACS, gating on CD3ε$^-$/NK1.1$^+$ cells (n = 3 or 4). (**C**) Expression of CD69 on the surface of NK cells. WT (+/+) and *Inam*$^{-/-}$ (−/−) mice were i.p. injected with 200 μg polyI:C or PBS. After 0, 3, and 24 h, CD69 expression was assayed by FACS, and the data were quantitatively analyzed using mean fluorescence intensity (MFI), gating on CD3ε$^-$/NK1.1$^+$ cells (n = 3). The data shown are representative of at least two independent experiments. Data are means ± SD of three independent samples. *$p < 0.05$.

after polyI:C stimulation, we performed ELISA and qPCR analysis of serum and spleen cells from WT and *Inam*$^{-/-}$ mice. However, protein levels of IL12p40, IFN-α, and IFN-β were not affected by *Inam* disruption in mice (Supplemental Fig. 2B). Additionally, mRNA expression of *Il-15* and *Il-18* genes was not decreased in *Inam*$^{-/-}$ mice (Supplemental Fig. 2C). These results suggest that INAM plays a critical role in the CD69 expression and rapid IFN-γ production, but not the cytotoxicity, of NK cells in response to polyI:C in a cytokine-independent manner.

INAM is required for the antimetastatic effect by polyI:C-based cancer immunotherapy

Malignant melanomas are one of the most important targets of NK-mediated cancer immunotherapy (27). In this study, we tested two types of polyI:C-based cancer immunotherapy model using B16D8 and B16F10 cell lines. NK cells show high cytotoxicity activity against B16D8 cells established in our laboratory as a subline of the B16 melanoma cell line (28). This subline was characterized by its low or virtually absent metastatic properties when injected s.c. into syngeneic C57BL/6 mice. In contrast, the B16F10 subline was characterized by its high metastatic capacity